

OBSERVATIONAL CONSTRAINTS ON THE TILTED SPATIALLY-FLAT AND THE UNTILTED NONFLAT ϕ CDM DYNAMICAL DARK ENERGY INFLATION MODELS

CHAN-GYUNG PARK^{1,2} AND BHARAT RATRA²

(Dated: April 29, 2019)
Draft version April 29, 2019

ABSTRACT

We constrain spatially-flat tilted and nonflat untilted scalar field (ϕ) dynamical dark energy inflation (ϕ CDM) models by using Planck 2015 cosmic microwave background (CMB) anisotropy measurements and recent baryonic acoustic oscillation distance observations, Type Ia supernovae apparent magnitude data, Hubble parameter measurements, and growth rate data. We assume an inverse power-law scalar field potential energy density $V(\phi) = V_0\phi^{-\alpha}$. We find that the combination of the CMB data with the four non-CMB data sets significantly improves parameter constraints and strengthens the evidence for nonflatness in the nonflat untilted ϕ CDM case from 1.8σ for the CMB measurements only to more than 3.1σ for the combined data. In the nonflat untilted ϕ CDM model current observations favor a spatially closed universe with spatial curvature contributing about two-thirds of a percent of the present cosmological energy budget. The flat tilted ϕ CDM model is a 0.4σ better fit to the data than is the standard flat tilted Λ CDM model: current data allow for the possibility that dark energy is dynamical. The nonflat tilted ϕ CDM model is in better accord with the Dark Energy Survey bounds on the rms amplitude of mass fluctuations now (σ_8) as a function of the nonrelativistic matter density parameter now (Ω_m) but it does not provide as good a fit to the larger-multipole Planck 2015 CMB anisotropy data as does the standard flat tilted Λ CDM model. A few cosmological parameter value measurements differ significantly when determined using the tilted flat and the untilted nonflat ϕ CDM models, including the cold dark matter density parameter and the reionization optical depth.

Subject headings: cosmological parameters — cosmic background radiation — large-scale structure of universe — inflation — observations — methods:statistical

1. INTRODUCTION

In the standard flat Λ CDM cosmogony (Peebles 1984) the cosmological energy budget is currently dominated by the cosmological constant Λ , which is responsible for powering the currently accelerated cosmological expansion.³ This standard Λ CDM model is consistent with most observational constraints, including CMB anisotropy measurements (Planck Collaboration 2016), baryonic acoustic oscillations (BAO) distance observations (Alam et al. 2017; Ryan et al. 2018), Type Ia supernova (SNIa) apparent magnitude data (Scolnic et al. 2017), and Hubble parameter measurements (Farooq et al. 2017; Yu et al. 2018),

The standard flat Λ CDM inflation cosmogony is characterized by six cosmological parameters usually picked to be: $\Omega_c h^2$ and $\Omega_b h^2$, the current values of the cold dark matter and baryonic matter density parameters multiplied by the square of the Hubble constant H_0 (in units of $100 \text{ km s}^{-1} \text{ Mpc}^{-1}$); A_s and n_s , the amplitude and spectral index of the primordial fractional energy density inhomogeneity power-law power spectrum; θ_{MC} , the angular size of the sound horizon at recombination; and τ , the reionization optical depth.

While the standard Λ CDM model assumes flat spatial geometry, current observational data allow for slightly curved

spatial hypersurfaces. Current measurements also allow a dark energy density that decreases slowly in time (and so also varies weakly spatially) and do not require a space- and time-independent Λ . Theoretically, it seems easier to accommodate dynamical dark energy than a Λ .

XCDM is a simple and widely used dynamical dark energy parameterization. Here the equation of state relating the dark energy fluid pressure and energy density is $p_X = w\rho_X$ where w is the equation of state parameter and the additional seventh cosmological parameter. XCDM does not provide a consistent description of the evolution of energy density spatial inhomogeneities and so is not a physically consistent description of dark energy. The simplest physically consistent dynamical dark energy model is ϕ CDM (Peebles & Ratra 1988; Ratra & Peebles 1988). In this model the dynamical dark energy is a scalar field ϕ with potential energy density $V(\phi) \propto \phi^{-\alpha}$ and $\alpha > 0$ is the additional seventh cosmological parameter.⁴

There have been a number of suggestions that some measurements favor dynamical dark energy over a Λ (Sahni et al. 2014; Ding et al. 2015; Solà et al. 2015; Zheng et al. 2016; Solà et al. 2017a, 2018, 2017b; Zhao et al. 2017; Solà et al. 2017c; Zhang et al. 2017a; Solà et al. 2017d; Gómez-Valent & Solà 2017; Cao et al. 2018; Gómez-Valent & Solà 2018). These analyses made a number of simplifying assumptions, either ignoring CMB anisotropy data, or only approximately accounting for it, or using it in the context of a generalized XCDM parameterization of dynamical dark energy. Some of

¹ Division of Science Education and Institute of Fusion Science, Chonbuk National University, Jeonju 54896, South Korea; e-mail: park.chan.gyung@gmail.com

² Department of Physics, Kansas State University, 116 Cardwell Hall, Manhattan, KS 66506, USA

³ For reviews of the standard model see Ratra & Vogeley (2008), Martin (2012), Brax (2018), and Luković et al. (2018). In this model, cold dark matter (CDM) and baryonic matter, both nonrelativistic, are the second and third largest contributors to the current cosmological energy budget; earlier they dominated over Λ and were responsible for decelerating the cosmological expansion.

⁴ Many cosmological data sets have been used to place constraints on the ϕ CDM model (see, e.g., Samushia et al. 2007; Yashar et al. 2009; Samushia & Ratra 2010; Chen & Ratra 2011b; Campanelli et al. 2012; Avsajanishvili et al. 2015; Solà et al. 2017b,c; Zhai et al. 2017; Sangwan et al. 2018, and references therein).

these analyses also include a high H_0 value determined from the local expansion rate in the data collections they use to investigate dark energy dynamics.⁵

Ooba et al. (2018c) have more exactly analyzed the Planck CMB data (as well as a few BAO distance measurements) by using the seven parameter spatially-flat Λ CDM and ϕ CDM dynamical dark energy tilted inflation models and discovered that both were weakly favored by the data, compared to the standard six parameter flat Λ CDM model, by 1.1σ and 1.3σ for the Λ CDM and ϕ CDM cases.⁶ These are not significant improvements over the standard flat Λ CDM case, but current data allow for the possibility that dark energy is dynamical. Furthermore, both dynamical dark energy models decrease the tension between the Planck CMB and the weak lensing observational bounds on σ_8 , the current value of rms fractional energy density inhomogeneity averaged over $8h^{-1}$ Mpc radius spheres.

Nonflat models have a characteristic length set by the non-vanishing spatial curvature and an energy density inhomogeneity power spectrum in a nonflat model that does not fully account for this spatial curvature length scale (as was done in the analyses of nonflat models by Planck Collaboration 2016) is not physically consistent. Nonflat cosmological inflation models are the only known way of defining physically consistent fractional energy density inhomogeneity power spectra in nonflat models. For open geometries the open-bubble inflation model (Gott 1982) is used to derive the non-power-law power spectrum (Ratra & Peebles 1994, 1995). For closed geometries the Hawking prescription for the initial state of the universe (Hawking 1984; Ratra 1985) defines a closed inflation model that is used to compute the non-power-law power spectrum (Ratra 2017). Unlike in the flat inflation case, there is no simple way to also accommodate tilt in nonflat inflation models. In the nonflat case n_s is no longer a free parameter but is instead replaced by the current spatial curvature density parameter Ω_k .

Ooba et al. (2018a) used this physically consistent nonflat un-tilted model non-power-law power spectrum of energy density spatial inhomogeneities in analyses of the Planck 2015 CMB anisotropy measurements (Planck Collaboration 2016) and found that these data do not require flat spatial geometry in the six parameter nonflat un-tilted Λ CDM inflation model.⁷ Park & Ratra (2018a,b) confirmed the results of Ooba et al. (2018a) by using the largest compilation of reliable observational data to study the nonflat un-tilted Λ CDM inflation model, and found stronger evidence for non-flatness, 5.2σ , favoring a very slightly closed model. The Planck 2015 CMB anisotropy data also do not require flat spatial surfaces in the seven parameter nonflat un-tilted Λ CDM dynamical dark energy inflation parameterization (Ooba et al. 2017). In the

⁵ We exclude this high local H_0 value from the data we use here to constrain cosmological model parameters, as it is inconsistent with the other data sets we utilize for this purpose, in the models we study.

⁶ Park & Ratra (2018b) used a much larger compilation of non-CMB data in an analysis of the tilted flat Λ CDM parameterization, confirming the Ooba et al. (2018c) findings, but at a lower level of significance, 0.3σ instead of 1.1σ .

⁷ Non-CMB observations do not provide tight constraints on spatial curvature (Farooq et al. 2015; Chen et al. 2016; Yu & Wang 2016; L’Huillier & Shafieloo 2017; Farooq et al. 2017; Li et al. 2016; Wei & Wu 2017; Rana et al. 2017; Yu et al. 2018; Mitra et al. 2017; Ryan et al. 2018), with the recent exception of a collection of all of the most recent BAO, Hubble parameter, and SNIa data, which (weakly) favors closed spatial geometry (Park & Ratra 2018c), as well as a recent collection of deuterium abundances that favor flat spatial hypersurfaces (Penton et al. 2018).

Λ CDM parameterization w is the seventh cosmological parameter with n_s again replaced by Ω_k . Using a much larger compilation of non-CMB data, Park & Ratra (2018b) confirmed the Ooba et al. (2017) results with higher significance: in the un-tilted nonflat Λ CDM case the data favor a closed model at 3.4σ significance and favor dynamical dark energy over a cosmological constant at 1.2σ significance. In the seven parameter nonflat un-tilted ϕ CDM dynamical dark energy inflation model (Pavlov et al. 2013) — with α as the seventh cosmological parameter — Ooba et al. (2018b) again discovered that Planck 2015 CMB anisotropy data do not demand flat spatial hypersurfaces. In both the Λ CDM and ϕ CDM dynamical dark energy inflation cases the data again favor a very mildly closed model. All three closed models are more compatible with weak lensing σ_8 constraints but do not fit the higher- ℓ C_ℓ data as well as the flat models do.

In this paper we determine observational limits on parameters of the seven parameter flat tilted ϕ CDM and the seven parameter nonflat un-tilted ϕ CDM dynamical dark energy inflation models. For this purpose, we use the same observational data in as Park & Ratra (2018b), the Planck CMB anisotropy, the Pantheon collection of 1048 SNIa apparent magnitudes (Scolnic et al. 2017), and a collection of BAO distances, Hubble parameters, and growth rates (see Park & Ratra 2018a,b for the data compilation and update).

We find that the seven parameter flat tilted ϕ CDM inflation model provides a better fit to these data than does the six parameter standard flat tilted Λ CDM model. However, for the larger compilation of data here the ϕ CDM dynamical dark energy inflation model is only 0.40σ better than the standard Λ CDM model (compared to the 1.3σ Ooba et al. 2018c found with their smaller data collection). While not a significant improvement over the standard model, the ϕ CDM model cannot be ruled out. In agreement with Ooba et al. (2018c) we also do not detect a deviation from $\alpha = 0$ (a cosmological constant) for the flat ϕ CDM model.⁸

Our results for the nonflat un-tilted ϕ CDM inflation model, derived using many more non-CMB observations, are consistent with and strengthen the Ooba et al. (2018b) conclusions. For the full data collection we use here we find a more than 3.1σ deviation from spatial flatness. The nonflat un-tilted ϕ CDM model better fits the weak lensing σ_8 – Ω_m bound. For the full data collection we use here (including CMB lensing data), the best-fit nonflat un-tilted ϕ CDM model has a reduced low- ℓ CMB temperature anisotropy multipole number (ℓ) power spectrum C_ℓ and is more compatible with the observations. However, overall the standard tilted flat Λ CDM model better fits the CMB data.⁹

These data determine H_0 in an almost model-independent way with a value that is compatible with most other estimates. As found in Park & Ratra (2018a,b), however, $\Omega_c h^2$ and τ differ significantly between the tilted flat and the un-tilted nonflat models and so care must be taken when utilizing cosmological measurements of such parameters.

⁸ These conclusions do not agree with those from earlier approximate analyses, based on less, as well as less reliable, data (Solà et al. 2017b,c), that favor the flat ϕ CDM model over the flat Λ CDM one by more than 3σ and find α deviating from 0 by more than 2σ .

⁹ As discussed elsewhere and below, the number of degrees of freedom of the Planck 2015 data are ambiguous and the nonflat un-tilted ϕ CDM model and the flat tilted Λ CDM model are not nested, thus it is impossible to translate the $\Delta\chi^2$ ’s we compute here to quantitative goodness of fit probabilities, consequently a large number of our statements about goodness of fit are qualitative. See below and see Park & Ratra (2018a,b) for more details about this issue.

In Sec. 2 we summarize the data sets we use in our analyses. In Sec. 3 we summarize the methods we use in our analyses here. Observational constraints following from these data for the flat tilted ϕ CDM and the nonflat untilted ϕ CDM inflation models are presented and discussed in Sec. 4. We summarize our main results in Sec. 5.

2. DATA

Following [Park & Ratra \(2018a,b\)](#) we utilize the Planck 2015 TT + lowP and TT + lowP + lensing CMB anisotropy measurements ([Planck Collaboration 2016](#)) to set bounds on the parameters of the ϕ CDM dynamical dark energy model. Here TT is the low- ℓ ($2 \leq \ell \leq 29$) and high- ℓ ($30 \leq \ell \leq 2508$; PlikTT) Planck temperature-only C_ℓ^{TT} angular power spectrum observations and lowP is the low- ℓ polarization C_ℓ^{TE} , C_ℓ^{EE} , and C_ℓ^{BB} angular power spectra measurements at $2 \leq \ell \leq 29$. The collection of low- ℓ CMB temperature and polarization power spectra is called lowTEB. The CMB lensing data we use is the measured Planck lensing potential power spectrum. The abbreviations TT + lowP and TT + lowP + lensing are used for the CMB data without and with CMB lensing data, respectively. The Planck collaboration recommends using the TT + lowP + lensing data combination as a conservative choice for parameter estimation (see the footnote to Table 4 of [Planck Collaboration 2016](#)).

The Type Ia supernova data set we use is the Pantheon set of 1048 SNIa apparent magnitude observations over the wide redshift (z) range of $0.01 < z < 2.3$ ([Scolnic et al. 2017](#)). This data set includes 276 SNIa ($0.03 < z < 0.65$ from the Pan-STARRS1 Medium Deep Survey and SNIa distance measurements from the SDSS, SNLS and low- z HST collections. We use the abbreviation SN to refer to the Pantheon sample.

We use the compilation of BAO data given in Table 1 of [Park & Ratra \(2018a\)](#). As in [Park & Ratra \(2018b\)](#), we use the updated BAO data point, $D_V(r_{d,\text{fid}}/r_d) = 3843 \pm 147$ Mpc of [Ata et al. \(2018\)](#), instead of the old value. See Sec. 2.3 of [Park & Ratra \(2018a\)](#) for more details. We note that the BAO data from BOSS DR12 ([Alam et al. 2017](#)) include growth rate ($f\sigma_8$) and radial BAO $H(z)$ data that are correlated with the other BOSS DR12 BAO measurements. We use the abbreviation BAO to refer to this BAO data compilation.

We also use the Hubble parameter, $H(z)$ (with 31 data points in total),¹⁰ and growth rate (with 10 points in total), $f(z)\sigma_8(z)$, observations of Tables 2 and 3 of [Park & Ratra \(2018a\)](#).

3. METHODS

In the ϕ CDM model we study here, the minimally coupled dark energy scalar field ϕ has an inverse power-law potential energy density

$$V(\phi) = V_0 \phi^{-\alpha} \quad (1)$$

with $\alpha > 0$ being a constant parameter and V_0 is determined in terms of α ([Peebles & Ratra 1988](#)). When α goes to zero, the dark energy behaves like the cosmological constant Λ .

We evolve a system of multiple components including radiation, neutrinos, matter, and the scalar field (that only directly

couples to the gravitational field). The evolution equations for the spatially homogeneous background and the spatial inhomogeneity linear perturbation variables are summarized in [Hwang & Noh \(2001, 2002\)](#). For the homogeneous background scalar field we use the initial conditions of [Peebles & Ratra \(1988\)](#) at scale factor $a_i = 10^{-10}$. This places the homogeneous background scalar field on the attractor/tracker solution ([Peebles & Ratra 1988](#); [Ratra & Peebles 1988](#); [Pavlov et al. 2013](#)).¹¹ As initial conditions of the spatially inhomogeneous scalar field perturbation and its time derivative, we take them to vanish in the CDM-comoving gauge (this is synchronous gauge without gauge modes) at $a_i = 10^{-10}$.¹²

For background evolution, we numerically solve the equation of motion of the scalar field,

$$\phi'' + \left(3 + \frac{\dot{H}}{H^2}\right) \phi' - \hat{V}_0 \alpha \phi^{-\alpha-1} \left(\frac{H_0}{H}\right)^2 = 0, \quad (2)$$

where $\phi' \equiv d\phi/d \ln a$, $H = \dot{a}/a$, $\hat{V}_0 \equiv V_0/H_0^2$, and an overdot denotes the time derivative d/dt . For the matter and dark energy dominated epochs, the normalized Hubble parameter $H(a)$ can be written as

$$\left(\frac{H}{H_0}\right)^2 = \frac{1}{1 - \frac{1}{6}(\phi')^2} \left[\Omega_m a^{-3} + \Omega_k a^{-2} + \frac{1}{3} \hat{V}_0 \phi^{-\alpha} \right], \quad (3)$$

where Ω_m and Ω_k are present values of the matter and curvature density parameters, respectively, and we have chosen units such that $8\pi G \equiv 1$. In actual calculations of Eq. (3), we have taken into account the contribution of photons as well as massless and massive neutrinos. Given cosmological parameters and initial conditions for the scalar field, we adjust the value of \hat{V}_0 to satisfy the condition $H/H_0 = 1$ at the present epoch ($a_0 = 1$) by applying the bisection method.

To estimate the likelihood distributions of ϕ CDM model parameters, we use the CAMB/COSMOMC package (Nov. 2016 version) ([Challinor & Lasenby 1999](#); [Lewis et al. 2000](#); [Lewis & Bridle 2002](#)). CAMB is used to compute the theoretical CMB temperature anisotropy, polarization, and lensing potential power spectra, as well as the matter density power spectrum, by solving for the evolution of the cosmological spatial inhomogeneity linear perturbations. COSMOMC determines model parameter values that are favored by the observational data by using the Markov chain Monte Carlo (MCMC) method. Since the current version of CAMB/COSMOMC package cannot be applied to scalar field dynamical dark energy models, we generalized CAMB by including the dynamical equations of motion for the spatially homogeneous background and spatial inhomogeneity linear perturbation quantities for the scalar field inverse power-law potential energy density model. CAMB uses the RECFAST routine to compute the recombination history of the universe ([Seager et al. 1999](#); [Wong et al. 2008](#)). We modified RECFAST to use the background evolution of the ϕ CDM model. We also altered the COSMOMC parameter interface to use the

¹¹ As a consequence of there being an attractor/tracker solution of the background scalar field nonlinear equation of motion (coupled to the Friedmann equation), the long-term time evolution is independent of the chosen initial conditions. However, there can be differences caused by different approaches from different initial conditions to the attractor/tracker solution and future data might require a more careful study of initial conditions effects.

¹² The evolution of spatially inhomogeneous scalar field quantities linearly perturbed about the background attractor solution also show tracking behavior and so are largely independent of the choice of initial conditions ([Ratra & Peebles 1988](#); [Brax et al. 2000](#)).

¹⁰ Hubble parameters have been measured over a wide range of redshift, from the present epoch to well beyond the cosmological deceleration-acceleration transition redshift. They provide evidence that this transition occurred and they have been used to measure the redshift of this transition at roughly the value expected in standard Λ CDM and other dark energy models ([Farooq & Ratra 2013](#); [Farooq et al. 2013](#); [Capozziello et al. 2014](#); [Moresco et al. 2016](#); [Farooq et al. 2017](#); [Yu et al. 2018](#); [Jesus et al. 2018](#); [Haridasu et al. 2018b](#)).

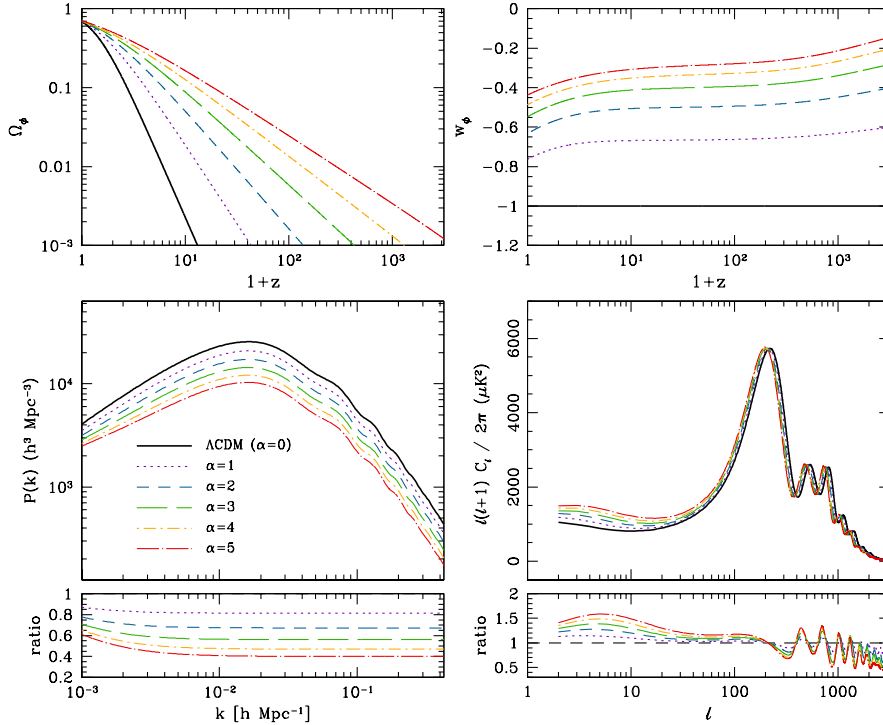


Figure 1. Top: Evolution of the dark energy scalar field density parameter (Ω_ϕ) and equation of state parameter (w_ϕ) in the tilted flat ϕ CDM model for integer values of α from 1 to 5. The black solid curve is for Λ CDM which corresponds to ϕ CDM with $\alpha = 0$. For these illustrations all other cosmological parameters are fixed to the mean values of the Λ CDM model parameters constrained by using the Planck 2015 CMB (TT + lowP) and the four non-CMB data sets (see Table 5 bottom-right panel of Park & Ratra 2018a). Bottom: Theoretical predictions for matter density and CMB temperature anisotropy angular power spectra in the ϕ CDM model at the corresponding α values. The ratios of the ϕ CDM model power spectra relative to the Λ CDM one are shown in the lower panels.

scalar field potential energy density parameter α as a new free parameter, in place of the constant equation of state parameter w of the XCDM model.

Unlike in the Λ CDM and XCDM analyses of Park & Ratra (2018a,b), here we use the Hubble constant H_0 as a new free parameter, instead of θ_{MC} (a default free parameter used in COSMOMC). There are two reasons for this change. First, θ_{MC} , the approximate angular size of the sound horizon at the decoupling epoch, is based on the fitting formula of the sound horizon size given in Hu & Sugiyama (1996) and is appropriate for models with a negligible level of dark energy in the early universe. In general, however, scalar field dark energy can be non-negligible at early times, depending on the scalar field potential energy density parameters and the initial conditions (e.g., see Park et al. 2014 for episodic domination of scalar field dark energy in the early universe). In the ϕ CDM model we study here a large value of α can result in a significant amount of dark energy at early times. Thus, a more accurate model parameterization is needed. Second, using the angular size of the sound horizon (θ) as a free parameter is less suitable in the presence of scalar field dark energy. Scalar field dark energy has its own dynamical equation that needs to be numerically evolved and so it is a matter of practical difficulty to adjust other cosmological parameter values along with the potential parameters of the scalar field to reproduce θ , a quantity that is obtained from an integration of the spatially homogeneous background equations of motion. The drawback of choosing the Hubble constant as a free parameter is that this makes it difficult to achieve MCMC convergence as the Hubble constant has degeneracy with spatial curvature and with the dark energy parameter α resulting in likelihood dis-

tributions that are degenerate and non-Gaussian.

Figure 1 shows the evolution of the scalar field dark energy density parameter (Ω_ϕ) and equation of state parameter ($w_\phi = p_\phi/\rho_\phi$, where p_ϕ and ρ_ϕ are the pressure and energy density of the scalar field) as well as theoretical predictions for matter density and CMB temperature anisotropy angular power spectra in the spatially-flat ϕ CDM model for some α values. The other cosmological parameters are fixed to the mean Λ CDM model parameters obtained by using the Planck 2015 CMB (TT + lowP) and the four non-CMB data sets (see the bottom-right panel of Table 5 in Park & Ratra 2018a). We can expect that the spatially-flat ϕ CDM model with large α can be excluded by CMB data alone. However, we will see that the nonflat ϕ CDM model with large values of α can be consistent with Planck CMB data.¹³

The primordial fractional energy density spatial inhomogeneity power spectrum in the tilted flat ϕ CDM inflation model (Lucchin & Matarrese 1985; Ratra 1992, 1989) is

$$P(k) = A_s \left(\frac{k}{k_0} \right)^{n_s}, \quad (4)$$

where k is wavenumber and A_s is the amplitude of the power spectrum at the pivot scale wavenumber $k_0 = 0.05 \text{ Mpc}^{-1}$. The corresponding power spectrum in the nonflat untilted ϕ CDM

¹³ However, from the bottom-left panels of Figs. 1 and 4, we see that matter power spectrum measurements over a wide range of wavenumbers, such as those shown in Fig. 19 of Planck Collaboration (2018), exclude large α values.

inflation model (Ratra & Peebles 1995; Ratra 2017) is

$$P(q) \propto \frac{(q^2 - 4K)^2}{q(q^2 - K)}, \quad (5)$$

which becomes the $n_s = 1$ spectrum in the flat limit (when $K = 0$). For scalar-type perturbations, $q = \sqrt{k^2 + K}$ is the wavenumber where spatial curvature $K = -(H_0^2/c^2)\Omega_k$ and c is the speed of light. For the negative Ω_k closed model, normal modes are characterized by positive integers $\nu = qK^{-1/2} = 3, 4, 5, \dots$. For the nonflat model, we use $P(q)$ as the initial perturbation power spectrum and normalize its amplitude at k_0 to A_s .

Our analyses methods are those described in Sec. 3.2 of Park & Ratra (2018a) and Sec. 3 of Park & Ratra (2018b).

4. OBSERVATIONAL CONSTRAINTS

We constrain the tilted flat ϕ CDM model with seven cosmological parameters ($\Omega_b h^2$, $\Omega_c h^2$, H_0 , τ , A_s , n_s , and α) and the untilted nonflat ϕ CDM model with seven parameters ($\Omega_b h^2$, $\Omega_c h^2$, H_0 , Ω_k , τ , A_s , and α). The calibration and foreground model parameters of the Planck data are also constrained as nuisance parameters by the COSMOMC program. In all parameter constraint tables presented in this work we also list three derived parameters, θ_{MC} , Ω_m (present value of the non-relativistic matter density parameter), and σ_8 .

We use the COSMOMC settings adopted by the Planck team (Planck Collaboration 2016) and the same priors on the model parameters as well as the same values of the present CMB temperature ($T_0 = 2.7255$ K), the effective number of neutrino species ($N_{\text{eff}} = 3.046$), and one massive neutrino species (with mass $m_\nu = 0.06$ eV) as used in Park & Ratra (2018a,b). We set tophat priors on the scalar field potential energy density parameter $0 < \alpha < 10$ and on the Hubble constant $0.2 \leq h \leq 1.0$. However, as detailed below, constraining the nonflat ϕ CDM models using the Planck CMB data alone is a complicated task due to the highly degenerate and non-Gaussian likelihood distributions of H_0 , Ω_k , and α , that make it difficult for the MCMC chains to converge. In this case (for only the CMB TT + lowP and TT + lowP + lensing data alone analyses), we apply a more restrictive tophat prior on the Hubble constant, $0.45 \leq h \leq 1.0$, to achieve convergence of the MCMC chains in a reasonable amount of time (given our computational resources).

Our results for the flat tilted ϕ CDM model are given in Figs. 2 and 3 and Tables 1 and 2. The likelihood distributions for the TT + lowP (+ lensing) + SN + BAO data combination (ignoring or accounting for the CMB lensing data) are omitted in the figures since they are very similar to those for the TT + lowP (+ lensing) + SN + BAO + $H(z)$ combination.

The results for the flat tilted ϕ CDM model in the TT + lowP panel of Table 1 and in the TT + lowP + lensing panel in Table 2 agree well with the corresponding entries in Table 2 of Ooba et al. (2018c), except for the 2σ upper limit on α for the TT + lowP case where we find $\alpha < 1.49$ while Ooba et al. (2018c) give $\alpha < 1.1$. Ooba et al. (2018c) use CLASS (Blas et al. 2011) for computing the C_ℓ 's and Monte Python (Audren et al. 2013) for the MCMC analyses, so it is comforting that both our results agree well.

Tables 1 and 2 show that, when added to the Planck anisotropy data, for the flat tilted ϕ CDM cosmogony, the BAO distance observations are largely more constraining than the $f\sigma_8$, SN, or $H(z)$ data, except for α when the SN measurements are more restrictive than the BAO ones and for σ_8 in the TT + lowP + lensing case when again the SN measurements are more restrictive than the BAO ones. This is very similar

to the results of the XCDM analyses (Park & Ratra 2018b). As in the XCDM case, each of the four non-CMB data sets used with the CMB data provide approximately equally tight bounds on $\Omega_b h^2$, τ , and A_s . We also note that the full combination of CMB and non-CMB data sets gives a somewhat worse constraint on the potential energy density parameter α than does the CMB + SN case, because the BAO, $H(z)$, and $f\sigma_8$ data favor a wider range of α and so weaken the α constraint. For a similar reason, the combination of the CMB and SN + BAO + $H(z)$ data constrains α tighter than does the full data combination.

Next, we use the same observational data to explore and constrain the parameter space of untilted nonflat ϕ CDM models. For these models the MCMC parameter search using only the Planck CMB data (either TT + lowP or TT + lowP + lensing) is very slow because of the highly degenerate and non-Gaussian shape of the likelihood distributions of H_0 , Ω_k , and α . The overall shape of the likelihood function in the three dimensional space of these three parameters can be described as a sheet of bent paper. Thus the full likelihood distribution is not well approximated by a simple multivariate Gaussian function. In practical terms the problem is that the MCMC random walks in the parameter space that are usually determined by the square root of the covariance matrix of model parameters multiplied by a random number vector drawn from a Gaussian distribution does not properly propagate throughout the whole space but stays within a local maximum of the likelihood distribution.

The most dramatic feature of the nonflat ϕ CDM analyses is that for this model the CMB data poorly constrains α and is also consistent with large values of α , unlike in the spatially-flat ϕ CDM model.¹⁴ This phenomenon can be understood more easily by comparing CMB data parameter constraints for the nonflat ϕ CDM and XCDM models. Figure 4 shows several examples of the ϕ CDM model with large α 's that are consistent with the Planck CMB observations. Here the parameters of the nonflat ϕ CDM models were chosen from the unconverged MCMC output determined using the Planck TT + lowP data, for α 's near 2, 4, 6, 8, and 10 (shown in the three-dimensional view of the MCMC chains in the H_0 - Ω_k - α space of Fig. 5 below). The individual cosmological parameters of these five models are very different. All the models have small Hubble constant ($H_0 < 45$ km s⁻¹Mpc⁻¹) and are highly positively curved ($\Omega_k < 0$).¹⁵ From Fig. 4, we see that as α becomes larger ($\alpha \gtrsim 6$), the behavior of the equation of state parameter w_ϕ becomes less sensitive to the variation of α , and ϕ CDM asymptotically behaves like the $w \approx -0.15$ XCDM parameterization for $z < 1000$. As shown in Fig. 5 (top-right panel), untilted nonflat XCDM parameterizations with $w \approx -0.15$ are consistent with Planck TT + lowP data for small Hubble constant and highly negative Ω_k . A similar thing happens in the nonflat ϕ CDM model for large values of α , and ϕ CDM models with very large α around 10 still have CMB power spectra that are consistent with the Λ CDM prediction (black curve in Fig. 4) within observational precision. However, as shown in the matter power spectra panel of Fig. 4, these ϕ CDM models are excluded by large-scale structure

¹⁴ α governs the dynamics of dark energy and when spatial curvature is allowed to vary this weakens the constraints on dark energy dynamics from any data set (see, e.g., Farooq et al. 2017, and references therein).

¹⁵ For example, for the nonflat ϕ CDM model with $\alpha \approx 10$, which corresponds to the red curves in Fig. 4, the parameters are $\Omega_b h^2 = 0.0022946$, $\Omega_c h^2 = 0.10990$, $\Omega_\nu h^2 = 6.4514 \times 10^{-7}$, $\Omega_k = -0.2023$, $\alpha = 9.795$, $\tau = 0.1123$, and $A_s = 2.2921 \times 10^{-9}$ (at $k_0 = 0.05$ Mpc⁻¹).

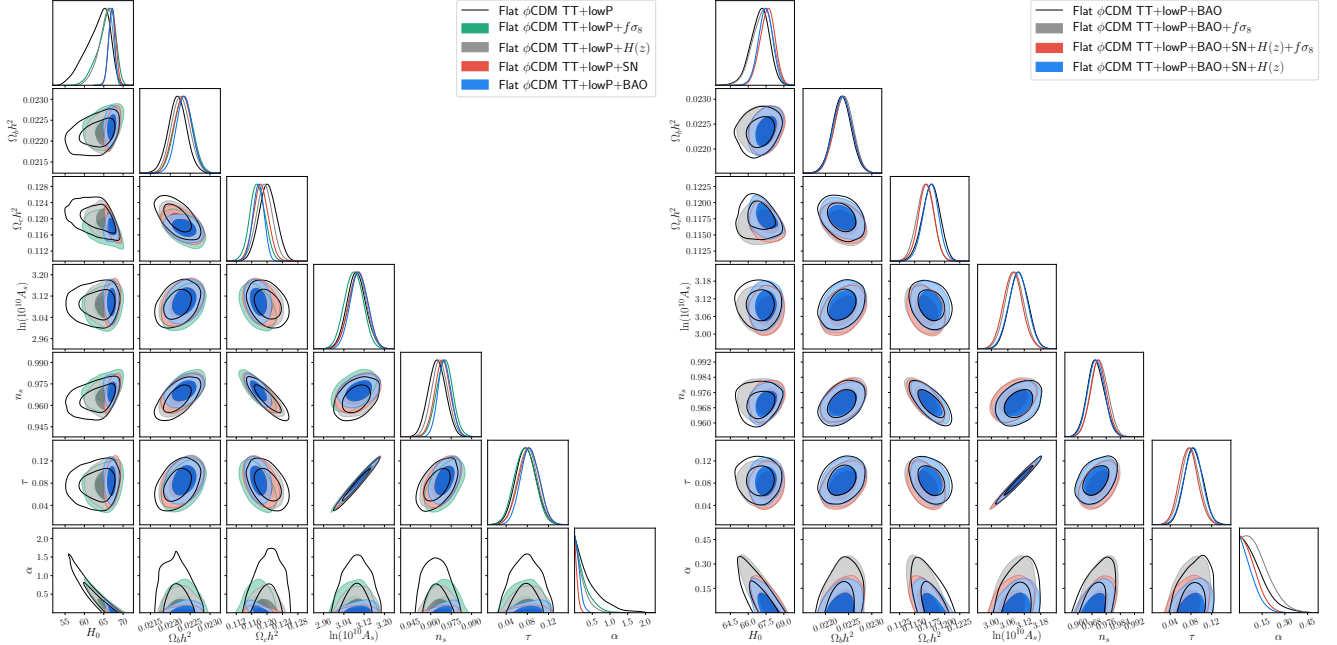


Figure 2. Likelihood distributions of the tilted flat ϕ CDM model parameters constrained by using Planck CMB TT + lowP, SN, BAO, $H(z)$, and $f\sigma_8$ data. Two-dimensional marginalized likelihood constraint contours and one-dimensional likelihoods are plotted for when each set of non-CMB data is combined with the Planck TT + lowP measurements (left panel) and when the growth rate, Hubble parameter, and SN data, as well as their combination, are combined with the TT + lowP + BAO data (right panel). For viewing clarity, the cases of TT + lowP (left) and TT + lowP + BAO (right panel) are shown with solid black curves.

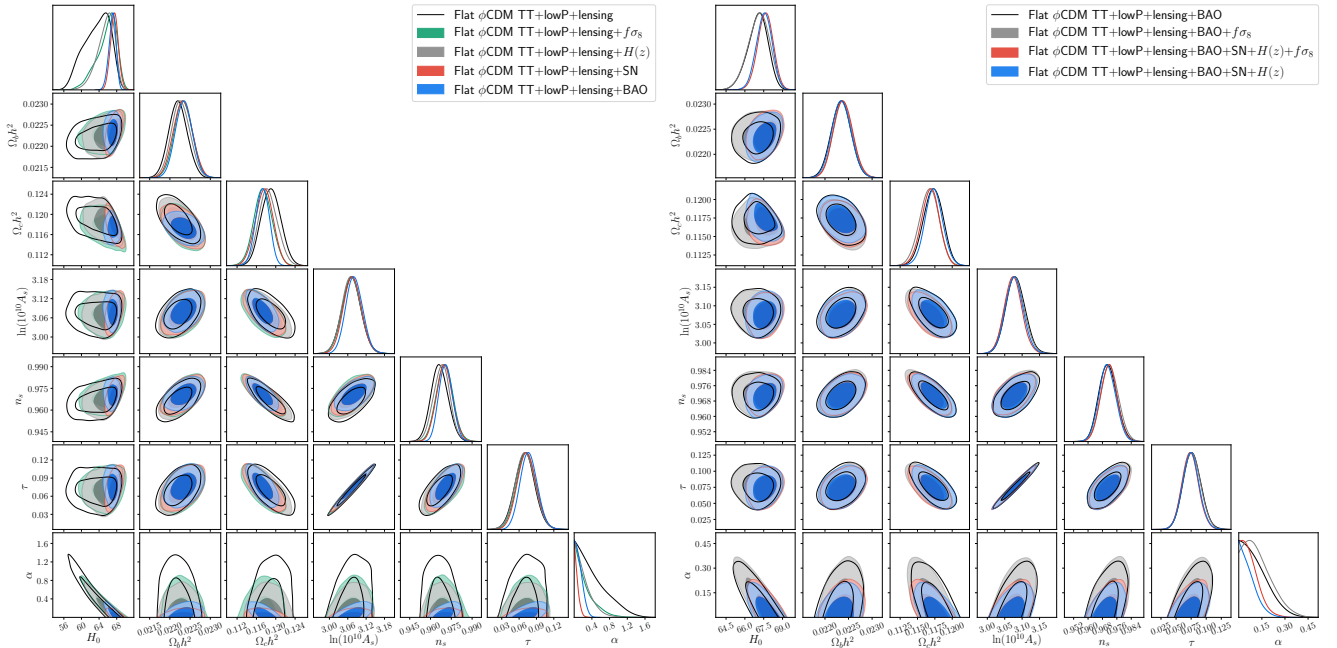


Figure 3. Same as Fig. 2 but now also accounting for the Planck CMB lensing data.

observations.

Figure 5 (top-left panel) shows the likelihood distributions of the untilted nonflat ϕ CDM model parameters constrained by using the Planck TT + lowP (red) and TT + lowP + lensing (blue) data. These are approximate estimates based on several sets of unconverged MCMC chains. For comparison we present results for the untilted nonflat XCDM parameterization parameters in the top-right panel. Here we use MCMC chain elements computed for dark energy equation of state parameter $w > -1$ to derive likelihood contours of

nonflat XCDM model parameters. Thus the resulting likelihood distributions differ from those obtained from the full MCMC outputs presented in Park & Ratra (2018b). The bottom panels show three-dimensional views of some selected untilted nonflat ϕ CDM model MCMC chains corresponding to parameter values that are consistent with the Planck TT + lowP (red dots) and TT + lowP + lensing (blue dots) data. The likelihood isosurfaces in the H_0 - Ω_k - α space appear to be long, thin, and curved, which means that the three parameters are highly degenerate and the likelihood functions are non-

Table 1
Tilted flat ϕ CDM model parameters constrained by using Planck TT + lowP, SN, BAO, $H(z)$, and $f\sigma_8$ data (mean and 68.3% confidence limits).

Parameter	TT+lowP	TT+lowP+SN	TT+lowP+BAO
$\Omega_b h^2$	0.02218 ± 0.00023	0.02231 ± 0.00023	0.02235 ± 0.00021
$\Omega_c h^2$	0.1202 ± 0.0023	0.1184 ± 0.0019	0.1177 ± 0.0015
H_0 [km s ⁻¹ Mpc ⁻¹]	63.3 ± 3.1	67.20 ± 0.91	66.97 ± 0.80
τ	0.077 ± 0.019	0.083 ± 0.019	0.085 ± 0.018
$\ln(10^{10} A_s)$	3.089 ± 0.037	3.097 ± 0.037	3.100 ± 0.035
n_s	0.9646 ± 0.0064	0.9686 ± 0.0058	0.9702 ± 0.0049
α [95.4% C.L.]	< 1.49	< 0.19	< 0.32
$100\theta_{MC}$	1.04063 ± 0.00049	1.04084 ± 0.00046	1.04095 ± 0.00043
Ω_m	0.359 ± 0.039	0.313 ± 0.012	0.3139 ± 0.0085
σ_8	0.791 ± 0.032	0.822 ± 0.016	0.816 ± 0.016
Parameter	TT+lowP+ $H(z)$	TT+lowP+SN+BAO	TT+lowP+SN+BAO+ $H(z)$
$\Omega_b h^2$	0.02226 ± 0.00023	0.02236 ± 0.00020	0.02237 ± 0.00020
$\Omega_c h^2$	0.1193 ± 0.0021	0.1177 ± 0.0013	0.1177 ± 0.0013
H_0 [km s ⁻¹ Mpc ⁻¹]	65.4 ± 1.9	67.44 ± 0.59	67.45 ± 0.61
τ	0.080 ± 0.019	0.084 ± 0.017	0.084 ± 0.018
$\ln(10^{10} A_s)$	3.094 ± 0.036	3.098 ± 0.034	3.098 ± 0.035
n_s	0.9666 ± 0.0061	0.9704 ± 0.0045	0.9704 ± 0.0046
α [95.4% C.L.]	< 0.68	< 0.19	< 0.20
$100\theta_{MC}$	1.04075 ± 0.00047	1.04093 ± 0.00043	1.04096 ± 0.00042
Ω_m	0.334 ± 0.022	0.3094 ± 0.0069	0.3093 ± 0.0070
σ_8	0.808 ± 0.022	0.820 ± 0.014	0.819 ± 0.015
Parameter	TT+lowP+ $f\sigma_8$	TT+lowP+BAO+ $f\sigma_8$	TT+lowP+SN+BAO+ $H(z)$ + $f\sigma_8$
$\Omega_b h^2$	0.02233 ± 0.00023	0.02239 ± 0.00020	0.02238 ± 0.00020
$\Omega_c h^2$	0.1175 ± 0.0020	0.1168 ± 0.0014	0.1169 ± 0.0013
H_0 [km s ⁻¹ Mpc ⁻¹]	65.6 ± 2.3	67.17 ± 0.83	67.61 ± 0.62
τ	0.075 ± 0.019	0.079 ± 0.018	0.076 ± 0.018
$\ln(10^{10} A_s)$	3.079 ± 0.037	3.084 ± 0.034	3.079 ± 0.035
n_s	0.9701 ± 0.0060	0.9721 ± 0.0048	0.9716 ± 0.0046
α [95.4% C.L.]	< 0.85	< 0.33	< 0.21
$100\theta_{MC}$	1.04091 ± 0.00047	1.04103 ± 0.00042	1.04101 ± 0.00042
Ω_m	0.328 ± 0.026	0.3101 ± 0.0084	0.3062 ± 0.0069
σ_8	0.792 ± 0.024	0.805 ± 0.015	0.808 ± 0.014

Gaussian. Since the nonflat ϕ CDM model with small Hubble constant and large α will be excluded by other cosmological observations, from here on we set a more restrictive prior for the Hubble constant, $h \geq 0.45$, to guarantee reasonably rapid convergence of the MCMC chains (given our computational resources) for the CMB data alone analyses. Likelihood distributions from the CMB data alone analyses for the more restrictive Hubble constant prior are shown in Fig. 6. Note that for the Planck TT + lowP data the constraint on α seems tighter than for the case of the TT + lowP + lensing data. This is because the region of large α but small Hubble constant favored by TT + lowP data is excluded by the more restrictive Hubble constant prior.

Our results for the nonflat untilted ϕ CDM model are presented in Figs. 7 and 8 and Tables 3 and 4. As in the flat tilted ϕ CDM models, the likelihood distributions for TT + lowP (+ lensing) + SN + BAO data (ignoring or accounting for the CMB lensing data) are omitted in the figures since they are very similar to those for TT + lowP (+ lensing) + SN + BAO + $H(z)$ data.

The entries for the nonflat untilted ϕ CDM model in Table 3

(TT + lowP panel) and those in the Table 4 (TT + lowP + lensing panel) are very consistent with the corresponding entries in Table 1 of Ooba et al. (2018b).¹⁶ Ooba et al. (2018b) computed the C_ℓ 's by using CLASS (Blas et al. 2011) and used the Monte Python software package (Audren et al. 2013) for the MCMC analyses; it is reassuring that both sets of results agree well.

The parameter constraints are more interesting in the non-flat untilted ϕ CDM model than in the flat tilted case. The general behavior of the cosmological parameter constraints are similar to those in the Λ CDM model (Park & Ratra 2018b). When CMB lensing data are accounted for, Table 4, Planck CMB data with either $H(z)$, BAO, SN, or $f\sigma_8$ data, provide roughly equally tight constraints on $\Omega_b h^2$, $\Omega_c h^2$, and θ_{MC} , while CMB + BAO measurements provide the tightest limits on H_0 , τ , A_s , Ω_k , Ω_m , and σ_8 , with CMB + SN setting the tightest limits on α . We note that the full combination of CMB

¹⁶ The TT + lowP and TT + lowP + lensing entries in the original version of Ooba et al. (2018b) were incorrect because of a numerical error in their initial computation. Our comparison here is made to the corrected Ooba et al. (2018b) results.

Table 2Tilted flat ϕ CDM model parameters constrained by using Planck TT + lowP + lensing, SN, BAO, $H(z)$, and $f\sigma_8$ data (mean and 68.3% confidence limits).

Parameter	TT+lowP+lensing	TT+lowP+lensing+SN	TT+lowP+lensing+BAO
$\Omega_b h^2$	0.02221 ± 0.00023	0.02232 ± 0.00023	0.02235 ± 0.00021
$\Omega_c h^2$	0.1190 ± 0.0020	0.1176 ± 0.0018	0.1173 ± 0.0014
H_0 [km s ⁻¹ Mpc ⁻¹]	63.6 ± 2.9	67.48 ± 0.91	67.01 ± 0.80
τ	0.070 ± 0.017	0.073 ± 0.016	0.077 ± 0.015
$\ln(10^{10} A_s)$	3.072 ± 0.031	3.075 ± 0.029	3.081 ± 0.027
n_s	0.9667 ± 0.0062	0.9701 ± 0.0058	0.9710 ± 0.0049
α [95.4% C.L.]	< 1.20	< 0.19	< 0.32
$100\theta_{MC}$	1.04076 ± 0.00047	1.04095 ± 0.00045	1.04100 ± 0.00042
Ω_m	0.353 ± 0.035	0.309 ± 0.011	0.3125 ± 0.0082
σ_8	0.780 ± 0.026	0.810 ± 0.010	0.805 ± 0.011
Parameter	TT+lowP+lensing+ $H(z)$	TT+lowP+lensing+SN+BAO	TT+lowP+lensing+SN+BAO+ $H(z)$
$\Omega_b h^2$	0.02227 ± 0.00023	0.02234 ± 0.00021	0.02235 ± 0.00020
$\Omega_c h^2$	0.1184 ± 0.0020	0.1174 ± 0.0013	0.1173 ± 0.0013
H_0 [km s ⁻¹ Mpc ⁻¹]	65.5 ± 2.0	67.52 ± 0.61	67.53 ± 0.62
τ	0.071 ± 0.017	0.074 ± 0.013	0.075 ± 0.014
$\ln(10^{10} A_s)$	3.072 ± 0.031	3.076 ± 0.024	3.078 ± 0.026
n_s	0.9681 ± 0.0060	0.9706 ± 0.0047	0.9708 ± 0.0046
α [95.4% C.L.]	< 0.73	< 0.20	< 0.20
$100\theta_{MC}$	1.04085 ± 0.00045	1.04098 ± 0.00041	1.04098 ± 0.00043
Ω_m	0.331 ± 0.023	0.3080 ± 0.0069	0.3078 ± 0.0071
σ_8	0.794 ± 0.018	0.8092 ± 0.0097	0.8096 ± 0.0098
Parameter	TT+lowP+lensing+ $f\sigma_8$	TT+lowP+lensing+BAO+ $f\sigma_8$	TT+lowP+lensing+SN+BAO+ $H(z)$ + $f\sigma_8$
$\Omega_b h^2$	0.02233 ± 0.00022	0.02238 ± 0.00020	0.02238 ± 0.00020
$\Omega_c h^2$	0.1174 ± 0.0019	0.1167 ± 0.0014	0.1168 ± 0.0013
H_0 [km s ⁻¹ Mpc ⁻¹]	65.7 ± 2.3	67.09 ± 0.84	67.63 ± 0.62
τ	0.072 ± 0.017	0.076 ± 0.015	0.074 ± 0.014
$\ln(10^{10} A_s)$	3.073 ± 0.030	3.078 ± 0.027	3.074 ± 0.025
n_s	0.9702 ± 0.0060	0.9720 ± 0.0049	0.9715 ± 0.0045
α [95.4% C.L.]	< 0.85	< 0.34	< 0.22
$100\theta_{MC}$	1.04092 ± 0.00046	1.04101 ± 0.00042	1.04101 ± 0.00042
Ω_m	0.327 ± 0.026	0.3106 ± 0.0084	0.3059 ± 0.0068
σ_8	0.789 ± 0.021	0.801 ± 0.011	0.8055 ± 0.0098

and non-CMB data results in somewhat weaker constraints on α (compared to the CMB + SN case) and on $\Omega_b h^2$ (compared to the CMB + $f\sigma_8$ case).

Let us focus on the results for CMB TT + lowP + lensing data, presented in Figs. 3 and 8 and Tables 2 and 4, where we see that adding in turn each of the four sets of non-CMB measurements to the CMB measurements (left panels in the two figures) result in likelihood contours that are quite compatible with each other, as well as with the CMB alone contours, for both the flat tilted and the nonflat untilted ϕ CDM model. It might be significant that the four sets of non-CMB observations do not pull the CMB only contours in very different directions. This is also true for the flat tilted ϕ CDM model when CMB lensing data are ignored (left panel of Fig. 2). However, in the nonflat untilted ϕ CDM cosmogony without the lensing data each of the four sets of non-CMB data added to the CMB data (left panel of Fig. 7) push the results towards a smaller $|\Omega_k|$ (closer to flat space) and larger H_0 as well as slightly larger τ and A_s and slightly smaller $\Omega_b h^2$ than is preferred by the CMB data alone, but all five constraint contour sets are largely mutually compatible, except for the H_0 and Ω_k

constraints where the TT + lowP data alone results differ from those derived using TT + lowP in combination with any one of the four non-CMB data sets.

Although augmenting the CMB data with the BAO data typically results in the largest difference, each of the other three sets of non-CMB data also contribute. Considering the TT + lowP + lensing data, we see from Table 2 for the flat tilted ϕ CDM model that the H_0 error bar is reduced the most by the full compilation of measurements relative to the CMB + BAO observations compilation, followed by the Ω_m error bar decrease compared to the CMB + BAO data collection. For the nonflat untilted ϕ CDM model, from Table 4, the error bars that reduce the most when CMB (accounting for lensing) data are used in combination with the four sets of non-CMB data are those on Ω_m and H_0 (relative to the CMB + BAO combination).

Focusing again on the TT + lowP + lensing data, Tables 2 and 4, for the flat tilted ϕ CDM model, we see that augmenting the CMB data with the four non-CMB data sets most affects H_0 , Ω_m , $\Omega_c h^2$, and σ_8 , with the H_0 and σ_8 central values moving up by 1.4σ and 0.98σ and the Ω_m and $\Omega_c h^2$ central values

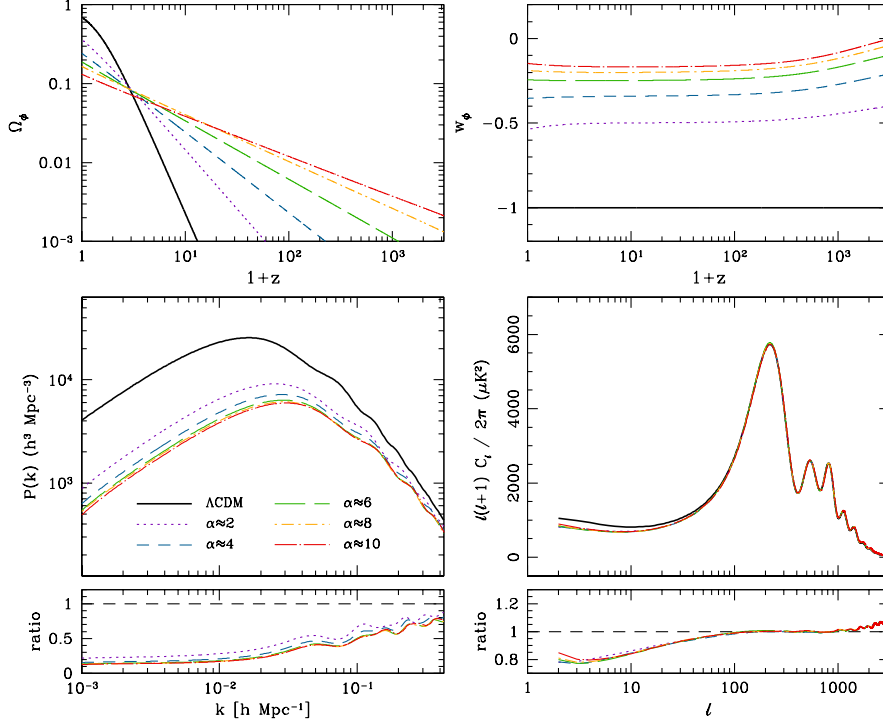


Figure 4. Top: Evolution of the dark energy scalar field density parameter (Ω_ϕ) and equation of state parameter (w_ϕ) for the untilted nonflat ϕ CDM model for various α values corresponding to the green dots in the bottom panels of Fig. 5. The black solid curve is for Λ CDM, whose model parameters are the same as in Fig. 1. The ϕ CDM models presented here were selected from the unconverged MCMC chains and are consistent with Planck observations. Bottom: Theoretical predictions for matter density and CMB temperature anisotropy angular power spectra for the ϕ CDM models.

moving down by 1.3σ and 1.1σ , all of the CMB data only error bars; $\ln(10^{10}A_s)$ is not much affected by including the four non-CMB sets of data, changing by only 0.065σ . The situation for the nonflat untilted ϕ CDM model is a little more dramatic, with H_0 and σ_8 central values moving up by 1.9σ and 1.7σ of the CMB data only error bars, Ω_m decreasing by 1.6σ , and Ω_k more closely approaching flatness by 1.5σ ; in this case the $\Omega_b h^2$ central value is not affected.

Figure 9 shows marginalized likelihood contours in the $\Omega_m - \alpha$ plane for the flat tilted ϕ CDM model and in $\alpha - \Omega_k$ plane for the nonflat untilted ϕ CDM case. For CMB TT + lowP + lensing measurements combined with the non-CMB observations, the flat ϕ CDM model prefers $\alpha = 0$, favoring the cosmological constant over dynamical dark energy. However, the nonflat ϕ CDM model, when constrained using all the data, prefers closed spatial hypersurfaces and also mildly prefers dynamical dark energy with scalar field potential energy density parameter $\alpha > 0$. Estimating 68.3% and 95.4% confidence limits of α using the information on the right-hand side with respect to the peak value (mode) in the marginalized 1-dimensional likelihood distribution, the mode $\pm 1\sigma$ (2σ) values for α are 0.113 ± 0.094 (0.19).

More precisely, including the four sets of non-CMB data, we discover in the tilted flat ϕ CDM model (bottom right panel of Table 2) that $\alpha < 0.22$ (at 2σ), which is more tightly restricted to $\alpha = 0$ and a cosmological constant than is the original Ooba et al. (2018c) finding of $\alpha < 0.28$ (at 2σ , the last column of their Table 2).¹⁷

However, perhaps the most interesting consequence of

adding in the four non-CMB data sets is the significant improvement of the evidence for nonflatness in the nonflat untilted ϕ CDM model, with it increasing to $\Omega_k = -0.0063 \pm 0.0020$, a more than 3.1σ deviation from flatness now, for the total data compilation in the bottom right panel of Table 4, compared to the 1.8σ away from flatness for the CMB only case. This is now accompanied by very mild evidence favoring dynamical dark energy, see the right panel of Fig. 9. This result is compatible with and strengthens that of Ooba et al. (2017) who found $\Omega_k = -0.006 \pm 0.003$ from Planck CMB data combined with a few BAO measurements. In favoring a closed geometry, the BAO measurements are the most important of the four non-CMB data sets.

From the total data combination (also accounting for CMB lensing data) in Tables 2 and 4, H_0 measured using the flat tilted and the nonflat untilted ϕ CDM models, 67.63 ± 0.62 and $67.36 \pm 0.72 \text{ km s}^{-1} \text{ Mpc}^{-1}$, are quite consistent with each other to within 0.28σ (of the quadrature sum of both the error bars). These values agree with the median statistics measurement $H_0 = 68 \pm 2.8 \text{ km s}^{-1} \text{ Mpc}^{-1}$ (Chen & Ratra 2011a), which agrees with earlier median statistics estimates (Gott et al. 2001; Chen et al. 2003). They are also compatible with many recent estimates of H_0 (L’Huillier & Shafieloo 2017; Chen et al. 2017; Luković et al. 2016; Wang et al. 2017; Lin & Ishak 2017; DES Collaboration 2017b; Yu et al. 2018; Haridasu et al. 2018a; Zhang et al. 2018; Gómez-Valent & Amendola 2018; Haridasu et al. 2018b; da Silva & Cavalcanti 2018; Zhang 2018), but, as is well known, they are lower than the local expansion rate estimate of $H_0 = 73.48 \pm 1.66 \text{ km s}^{-1} \text{ Mpc}^{-1}$ (Riess et al. 2018).¹⁸

We find that H_0 and σ_8 (see discussion below) are the only

¹⁷ These results do not agree with those of earlier approximate analyses that used less reliable, and less, data, and indicated evidence for α deviating from 0 by more than 2σ (Solà et al. 2017b,c).

¹⁸ This local expansion rate estimate is 3.3σ (3.4σ), of the quadrature sum

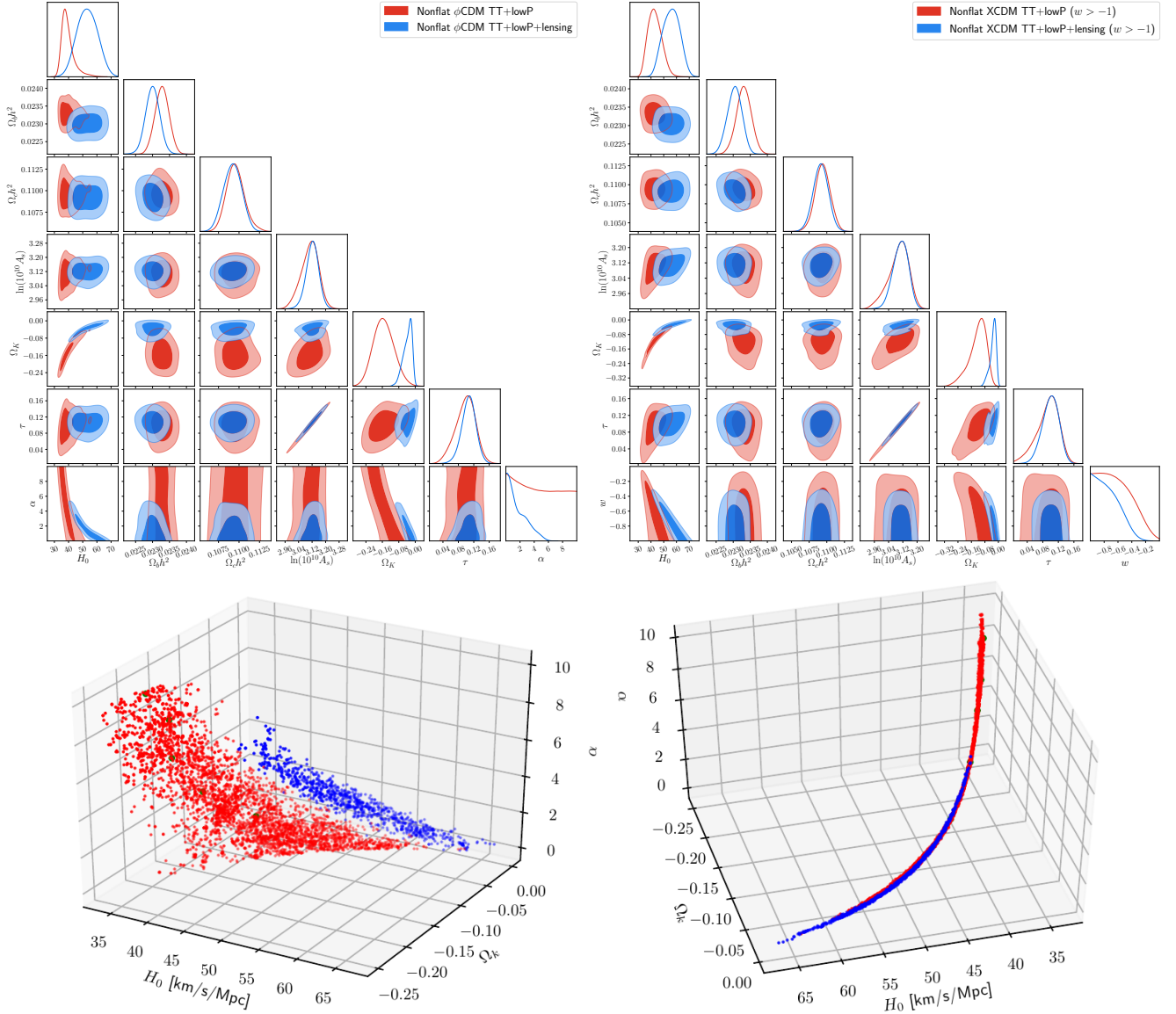


Figure 5. Top left: Comparison of likelihood distributions of the untitled nonflat ϕ CDM model parameters constrained using Planck CMB TT + lowP and TT + lowP + lensing data. Note that these likelihood distributions have been obtained from unconverged MCMC chains. Top right: Similar plot as in top-left panel but now for the untitled nonflat XCDM model (Park & Ratra 2018b). Here the likelihood distributions have been derived from MCMC chain elements computed for equation of state parameter $w > -1$. Bottom panels: Three-dimensional views of some selected untitled nonflat ϕ CDM model MCMC chain elements with $\Delta\chi^2 < 18$ relative to the minimum value (see Table 5 below), constrained using Planck TT + lowP (red dots) and TT + lowP + lensing (blue dots) data. The five green dots for the TT + lowP data indicate the position of the five untitled nonflat ϕ CDM models presented in Fig. 4.

measured parameters whose values are almost independent of the cosmological model (spatial curvature and tilt) used in the analysis. Measurements of other parameters determined by using the two ϕ CDM models differ more significantly. Specifically, measurements determined using the total data (also including CMB lensing) of Ω_m , θ_{MC} , $\ln(10^{10}A_s)$, $\Omega_b h^2$, τ , and $\Omega_c h^2$, differ by 1.4σ , 1.9σ , 2.3σ , 2.3σ , 2.6σ , and 4.6σ (of the quadrature sum of both the error bars). For some parameters, especially $\Omega_c h^2$ as well as possibly τ , $\Omega_b h^2$, and A_s , the model dependence of the value results in a much larger un-

of both the error bars, larger than the H_0 value measured here using the flat tilted ϕ CDM (nonflat untitled ϕ CDM) model. However, some other local expansion rate determinations find somewhat lower H_0 's with somewhat larger error bars (Rigault et al. 2015; Zhang et al. 2017b; Dhawan et al. 2017; Fernández Arenas et al. 2018); for related discussions see Roman et al. (2017), Kim et al. (2018), and Jones et al. (2018).

certainty than that due to the statistical uncertainty in the given cosmological model. This was first detected when comparing measurements made using the flat tilted Λ CDM and the nonflat untitled Λ CDM model (Park & Ratra 2018a) and is also present in the XCDM case (Park & Ratra 2018b). From Tables 2 and 4, for the total data collection (also including CMB lensing), we find in the tilted flat ϕ CDM (untitled nonflat ϕ CDM) case $0.046 \leq \tau \leq 0.102$ ($0.098 \leq \tau \leq 0.146$) and $0.02198 \leq \Omega_b h^2 \leq 0.02278$ ($0.02264 \leq \Omega_b h^2 \leq 0.02344$) at 2σ , which are almost disjoint, and $0.1142 \leq \Omega_c h^2 \leq 0.1194$ ($0.1073 \leq \Omega_c h^2 \leq 0.1113$), which are completely separated from each other. Current cosmological data cannot be used to measure $\Omega_c h^2$ or τ (and possibly some of the other cosmological parameters also) in a model independent way.

From the total data combination (also including CMB lensing data), σ_8 's measured using the two ϕ CDM models, Tables

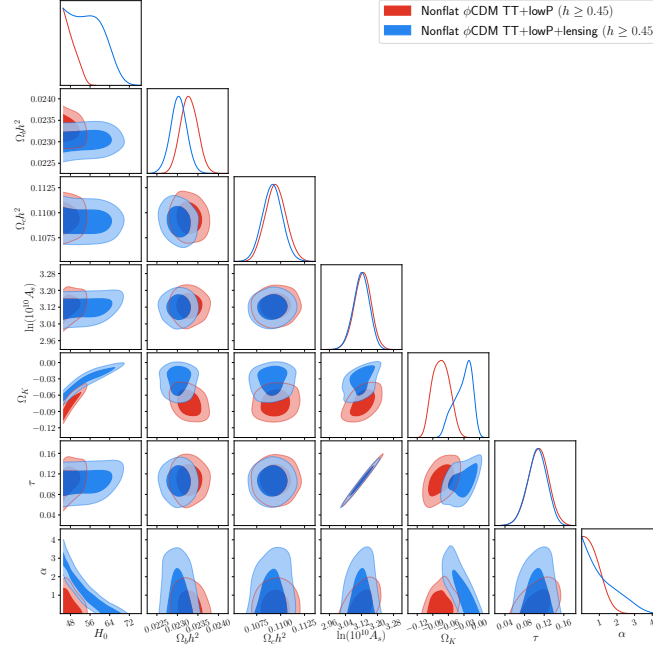


Figure 6. Likelihood distributions of the untilted nonflat ϕ CDM model parameters for the Planck CMB TT + lowP and TT + lowP + lensing data. Here we have used the more restrictive Hubble constant prior, $h \geq 0.45$. The MCMC processes have statistically converged.

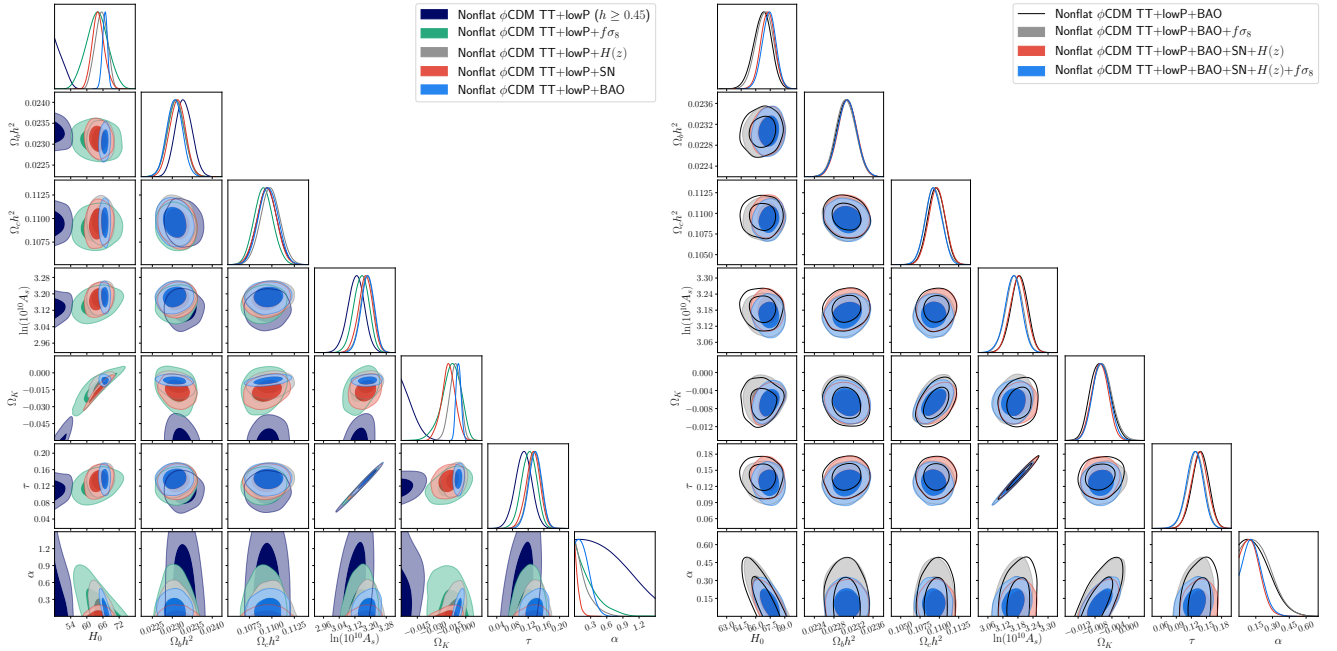


Figure 7. Likelihood distributions of the untilted nonflat ϕ CDM model parameters constrained using Planck CMB TT + lowP, SN, BAO, $H(z)$, and $f\sigma_8$ data sets. Two-dimensional marginalized likelihood constraint contours and one-dimensional likelihood distributions are plotted for when each set of non-CMB data is combined with the Planck TT + lowP data (left panel) and when the growth rate, Hubble parameter, and SN data, as well as their combination, are added to TT + lowP + BAO data (right panel). For clarity of viewing, the result of TT + lowP + BAO is shown with solid black curves in the right panel. The TT + lowP CMB data alone contours are derived using the more restrictive $h \geq 0.45$ prior.

2 and 4, agree to 0.034σ (of the quadrature sum of both the error bars). Figures 10 and 11 show the marginalized two-dimensional Ω_m - σ_8 likelihood contours for the flat tilted and nonflat untilted ϕ CDM models constrained using the CMB and non-CMB data. In each panel we also show the Λ CDM model constraints from a combined analysis of the first year galaxy clustering and weak lensing data of the Dark Energy Survey (DES Y1 All) (DES Collaboration 2017a), whose 1σ

confidence limits are $\Omega_m = 0.264^{+0.032}_{-0.019}$ and $\sigma_8 = 0.807^{+0.062}_{-0.041}$. The marginalized likelihood contours in the Ω_m - σ_8 plane derived by adding each of the four sets of non-CMB data in turn to the CMB data are consistent with each other. Here the BAO data provide the most stringent constraints among the four sets of non-CMB data.

Although the σ_8 constraints from the flat tilted and nonflat untilted ϕ CDM analyses (ignoring and accounting for CMB

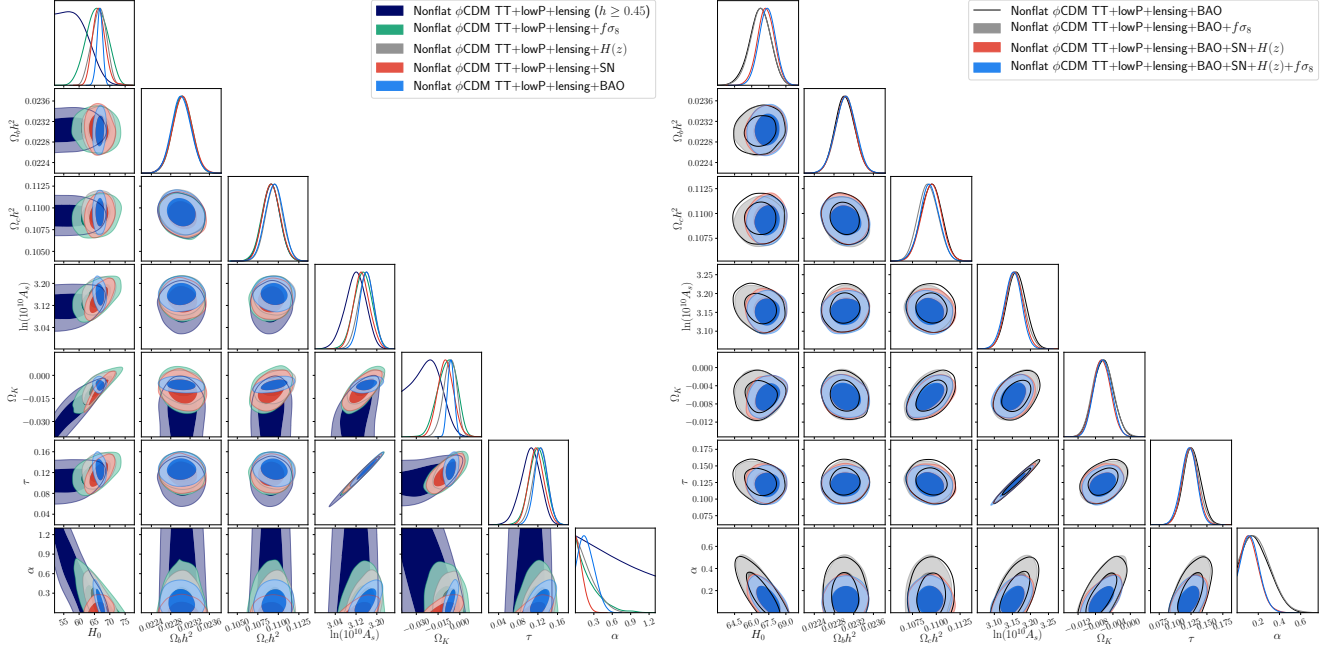


Figure 8. Same as Fig. 7 but now also accounting for the Planck CMB lensing data. The TT + lowP + lensing CMB data alone contours are derived using the more restrictive $h \geq 0.45$ prior.

lensing data) are consistent with the DES Y1 All measurements, the Ω_m bounds here prefer a larger value by about 1.3σ (of the quadrature sum of both the error bars) for the flat tilted ϕ CDM case for the total data collection. We note that the best-fit point of the nonflat untilted ϕ CDM model constrained by using the CMB data (also including lensing) combined with all non-CMB measurements enters inside the 1σ (68.3%) region of the DES Y1 All likelihood distribution (lower right panel of Fig. 11), unlike the case for the flat tilted ϕ CDM model (Fig. 10 lower right panel).

Table 5 lists χ^2 's for the best-fit flat tilted and nonflat untilted ϕ CDM models. The best-fit position in parameter space is found using Powell's minimization method, an efficient algorithm to locate the χ^2 minimum. We list the χ^2 contribution of each data set. The total χ^2 is the sum of the individual ones from the high- ℓ CMB TT likelihood (χ^2_{plikTT}), the low- ℓ CMB power spectra of temperature and polarization (χ^2_{lowTEB}), lensing (χ^2_{lensing}), SN (χ^2_{SN}), BAO (χ^2_{BAO}), $f\sigma_8$ ($\chi^2_{f\sigma_8}$), $H(z)$ data ($\chi^2_{H(z)}$), and from the foreground nuisance parameters (χ^2_{prior}). As a result of the nonstandard normalization of the Planck data likelihoods, the number of CMB degrees of freedom is ambiguous. Thus, the absolute value of χ^2 for the Planck CMB data is arbitrary, and only the relative difference between χ^2 of one model and another is meaningful for the Planck data. For the non-CMB data, the degrees of freedom are 10, 15, 31, 1042¹⁹ for the $f\sigma_8$, BAO, $H(z)$, SN observations, respectively, resulting in 1098 degrees of freedom all together. The reduced χ^2 's for the individual non-CMB data sets are $\chi^2/\nu \lesssim 1$. There are 189 points in the Planck TT + lowP (binned) CMB data anisotropy angular power spectrum and 197 points when the CMB lensing measurements are included.

In the last column of Table 5, we list $\Delta\chi^2$, the excess χ^2 of the best-fit seven parameter ϕ CDM model relative to the χ^2

¹⁹ This is the number of degrees of freedom for the flat Λ CDM model, given by the number of data points (1048) minus the number of parameters such as the matter density (Ω_m) and the five internal nuisance parameters.

of the related six parameter Λ CDM model that is constrained by using the same data combination. The minimum χ^2 values for the Λ CDM and XCDM models are presented in Tables 7 and 8 of Park & Ratra (2018b). These models are nested; the seven parameter flat tilted ϕ CDM (nonflat untilted ϕ CDM) model reduces to the six parameter flat tilted Λ CDM (nonflat untilted Λ CDM) model when α goes to zero.²⁰ Here the ambiguity in the number of Planck CMB data degrees of freedom is no longer an obstacle to converting the $\Delta\chi^2$ to a relative goodness of fit probability. From $\sqrt{-\Delta\chi^2}$, for the complete data (accounting for CMB lensing), for a single additional free parameter, we find that the flat tilted ϕ CDM (nonflat untilted ϕ CDM) model is a 0.40σ (0.93σ) better fit to the data than is the flat tilted Λ CDM (nonflat untilted Λ CDM) model.²¹ These findings are compatible with those of Ooba et al. (2018c) and Ooba et al. (2017).

Of all three flat cases, tilted flat ϕ CDM best fits the combined data (although there is no significant difference between all three cases), but at a lower level of significance than the 1.3σ found by Ooba et al. (2018c) using a very small sample of non-CMB data compared to what we have used here, and far from the 3 or 4σ result found in earlier approximate analyses by Solà et al. (2017b,c). While the tilted flat ϕ CDM and XCDM cases do not provide a much better fit to the data, available data allow for the possibility that dark energy is dynamical.

It is clear that relative to the flat models, in terms of $\Delta\chi^2$ values, the nonflat models do a worse job of fitting the higher-

²⁰ This is also true of the XCDM parameterization when the equation of state parameter w goes to -1 .

²¹ XCDM does not do as well as ϕ CDM, with the flat tilted XCDM (nonflat untilted XCDM) parameterization being a 0.28σ (0.87σ) better fit to the data than is the flat tilted Λ CDM (nonflat untilted Λ CDM) model (Park & Ratra 2018b). We emphasize that nonflat untilted Λ CDM does not fit as well as flat tilted Λ CDM, although as discussed in Ooba et al. (2018a, 2017, 2018b) and Park & Ratra (2018a,b), it is not known how to transform this into a relative probability because the Planck 2015 CMB data number of degrees of freedom is unavailable and the two six parameter models are not nested.

Table 3Untilted nonflat ϕ CDM model parameters constrained by using Planck TT + lowP, SN, BAO, $H(z)$, and $f\sigma_8$ data (mean and 68.3% confidence limits).

Parameter	TT+lowP ($h \geq 0.45$)	TT+lowP+SN	TT+lowP+BAO
$\Omega_b h^2$	0.02329 ± 0.00021	0.02313 ± 0.00020	0.02306 ± 0.00020
$\Omega_c h^2$	0.1095 ± 0.0011	0.1094 ± 0.0011	0.1096 ± 0.0011
H_0 [km s $^{-1}$ Mpc $^{-1}$]	48.4 ± 2.5	64.2 ± 2.3	66.68 ± 0.91
τ	0.108 ± 0.021	0.132 ± 0.018	0.138 ± 0.016
$\ln(10^{10} A_s)$	3.126 ± 0.042	3.174 ± 0.036	3.185 ± 0.033
Ω_k	-0.074 ± 0.016	-0.0162 ± 0.0064	-0.0067 ± 0.0023
α [95.4% C.L.]	< 1.81	< 0.20	< 0.46
$100\theta_{MC}$	1.04217 ± 0.00042	1.04209 ± 0.00042	1.04204 ± 0.00041
Ω_m	0.573 ± 0.057	0.324 ± 0.023	0.2999 ± 0.0086
σ_8	0.733 ± 0.026	0.819 ± 0.017	0.815 ± 0.017
Parameter	TT+lowP+ $H(z)$	TT+lowP+SN+BAO	TT+lowP+SN+BAO+ $H(z)$
$\Omega_b h^2$	0.02309 ± 0.00021	0.02306 ± 0.00019	0.02307 ± 0.00019
$\Omega_c h^2$	0.1098 ± 0.0011	0.1096 ± 0.0011	0.1097 ± 0.0011
H_0 [km s $^{-1}$ Mpc $^{-1}$]	65.3 ± 2.2	67.16 ± 0.70	67.24 ± 0.72
τ	0.136 ± 0.017	0.134 ± 0.016	0.136 ± 0.016
$\ln(10^{10} A_s)$	3.182 ± 0.035	3.178 ± 0.033	3.182 ± 0.033
Ω_k	-0.0100 ± 0.0052	-0.0073 ± 0.0020	-0.0068 ± 0.0019
α [95.4% C.L.]	< 0.60	< 0.28	< 0.29
$100\theta_{MC}$	1.04204 ± 0.00042	1.04202 ± 0.00041	1.04206 ± 0.00041
Ω_m	0.314 ± 0.022	0.2957 ± 0.0063	0.2952 ± 0.0066
σ_8	0.813 ± 0.022	0.819 ± 0.016	0.820 ± 0.016
Parameter	TT+lowP+ $f\sigma_8$	TT+lowP+BAO+ $f\sigma_8$	TT+lowP+SN+BAO+ $H(z)$ + $f\sigma_8$
$\Omega_b h^2$	0.02309 ± 0.00021	0.02304 ± 0.00020	0.02307 ± 0.00020
$\Omega_c h^2$	0.1091 ± 0.0010	0.1093 ± 0.0011	0.1092 ± 0.0011
H_0 [km s $^{-1}$ Mpc $^{-1}$]	63.8 ± 4.0	66.91 ± 0.91	67.37 ± 0.71
τ	0.122 ± 0.019	0.128 ± 0.017	0.126 ± 0.016
$\ln(10^{10} A_s)$	3.152 ± 0.039	3.164 ± 0.033	3.161 ± 0.033
Ω_k	-0.0136 ± 0.0090	-0.0063 ± 0.0023	-0.0065 ± 0.0020
α [95.4% C.L.]	< 0.86	< 0.46	< 0.30
$100\theta_{MC}$	1.04206 ± 0.00041	1.04204 ± 0.00042	1.04206 ± 0.00041
Ω_m	0.330 ± 0.042	0.2972 ± 0.0084	0.2930 ± 0.0062
σ_8	0.789 ± 0.028	0.805 ± 0.016	0.809 ± 0.015

ℓ C_ℓ 's than they do at fitting the lower- ℓ C_ℓ 's. However, the models are not nested so it is not possible to turn these differences into relative goodness of fit probabilities (as the number of degrees of freedom of the Planck 2015 data is ambiguous). We note that there have been studies on systematic differences between constraints determined from the higher- ℓ and the lower- ℓ Planck 2015 data (Addison et al. 2016; Planck Collaboration 2017). Also, in the tilted flat Λ CDM model, there seem to be inconsistencies between the higher- ℓ Planck and the South Pole Telescope CMB data (Aylor et al. 2017). Possibly, if these differences are real, when they are resolved this could result in a decrease of the $\Delta\chi^2$'s found here.

Figures 12 and 13 plot the CMB high- ℓ TT, and the low- ℓ TT, TE, EE power spectra of the best-fit flat tilted and nonflat untilted ϕ CDM dynamical dark energy inflation models, ignoring and accounting for the lensing data, respectively. The best-fit flat tilted ϕ CDM models favored by the CMB and non-CMB data are in good agreement with the observed CMB power spectra at all ℓ (this is also the case for the best-fit flat tilted XCDM parameterization, Park & Ratra 2018b). However, similar to the nonflat Λ CDM and XCDM cases studied

in Park & Ratra (2018a,b), the nonflat untilted ϕ CDM model constrained with the Planck 2015 CMB anisotropy data and each non-CMB data set generally provides a poorer fit to the low- ℓ EE power spectrum while it provides a better fit to the low- ℓ TT power spectrum (see the bottom left panel of Figs. 12 and 13). The best-fit C_ℓ model power spectra shapes relative to the Planck CMB data points are compatible with the χ^2 values listed in Table 5. For example, the best-fit untilted nonflat ϕ CDM model constrained by using the TT + lowP + $H(z)$ data has an EE power spectrum shape at low- ℓ that is most deviant from the Planck data and a corresponding value of $\chi^2_{\text{lowTEB}} = 10500.10$ that is larger by 3.69 relative to the best-fit tilted flat Λ CDM model $\chi^2_{\text{lowTEB}} = 10496.41$ for the TT + lowP data (see Table 5 here and Table 7 of Park & Ratra 2018b).

Figure 14 shows the best-fit primordial power spectra of fractional energy density spatial inhomogeneity perturbations for the nonflat untilted ϕ CDM model constrained by using the Planck TT + lowP (left) and TT + lowP + lensing (right panel) data together with the other non-CMB data sets. The low q region reduction in power in the best-fit closed untilted

Table 4Untilted nonflat ϕ CDM model parameters constrained by using Planck TT + lowP + lensing, SN, BAO, $H(z)$, and $f\sigma_8$ data (mean and 68.3% confidence limits).

Parameter	TT+lowP+lensing ($h \geq 0.45$)	TT+lowP+lensing+SN	TT+lowP+lensing+BAO
$\Omega_b h^2$	0.02303 ± 0.00020	0.02305 ± 0.00020	0.02302 ± 0.00020
$\Omega_c h^2$	0.1091 ± 0.0011	0.1092 ± 0.0011	0.1095 ± 0.0011
H_0 [km s $^{-1}$ Mpc $^{-1}$]	55.2 ± 6.1	66.5 ± 2.1	66.73 ± 0.93
τ	0.105 ± 0.020	0.117 ± 0.015	0.126 ± 0.014
$\ln(10^{10} A_s)$	3.118 ± 0.039	3.142 ± 0.031	3.161 ± 0.026
Ω_k	-0.032 ± 0.017	-0.0098 ± 0.0055	-0.0062 ± 0.0023
α [95.4% C.L.]	< 3.30	< 0.26	< 0.46
$100\theta_{MC}$	1.04213 ± 0.00041	1.04213 ± 0.00041	1.04210 ± 0.00041
Ω_m	0.45 ± 0.10	0.301 ± 0.018	0.2992 ± 0.0086
σ_8	0.716 ± 0.049	0.804 ± 0.014	0.803 ± 0.012
Parameter	TT+lowP+lensing+ $H(z)$	TT+lowP+lensing+SN+BAO	TT+lowP+lensing+SN+BAO+ $H(z)$
$\Omega_b h^2$	0.02303 ± 0.00020	0.02302 ± 0.00020	0.02303 ± 0.00020
$\Omega_c h^2$	0.1095 ± 0.0010	0.1094 ± 0.0011	0.1095 ± 0.0010
H_0 [km s $^{-1}$ Mpc $^{-1}$]	66.5 ± 2.4	67.16 ± 0.72	67.25 ± 0.74
τ	0.125 ± 0.015	0.122 ± 0.013	0.123 ± 0.012
$\ln(10^{10} A_s)$	3.158 ± 0.029	3.153 ± 0.025	3.155 ± 0.024
Ω_k	-0.0069 ± 0.0045	-0.0071 ± 0.0020	-0.0065 ± 0.0020
α [95.4% C.L.]	< 0.60	< 0.31	< 0.32
$100\theta_{MC}$	1.04210 ± 0.00041	1.04209 ± 0.00041	1.04209 ± 0.00042
Ω_m	0.302 ± 0.022	0.2950 ± 0.0064	0.2945 ± 0.0065
σ_8	0.801 ± 0.019	0.807 ± 0.011	0.807 ± 0.011
Parameter	TT+lowP+lensing+ $f\sigma_8$	TT+lowP+lensing+BAO+ $f\sigma_8$	TT+lowP+lensing+SN+BAO+ $H(z)$ + $f\sigma_8$
$\Omega_b h^2$	0.02304 ± 0.00019	0.02303 ± 0.00020	0.02304 ± 0.00020
$\Omega_c h^2$	0.1091 ± 0.0011	0.1091 ± 0.0010	0.1093 ± 0.0010
H_0 [km s $^{-1}$ Mpc $^{-1}$]	65.8 ± 3.4	66.77 ± 0.91	67.36 ± 0.72
τ	0.119 ± 0.017	0.125 ± 0.013	0.122 ± 0.012
$\ln(10^{10} A_s)$	3.146 ± 0.034	3.158 ± 0.026	3.152 ± 0.024
Ω_k	-0.0087 ± 0.0065	-0.0062 ± 0.0023	-0.0063 ± 0.0020
α [95.4% C.L.]	< 0.79	< 0.48	< 0.31
$100\theta_{MC}$	1.04209 ± 0.00041	1.04208 ± 0.00041	1.04210 ± 0.00041
Ω_m	0.309 ± 0.032	0.2981 ± 0.0084	0.2931 ± 0.0064
σ_8	0.792 ± 0.025	0.799 ± 0.012	0.805 ± 0.011

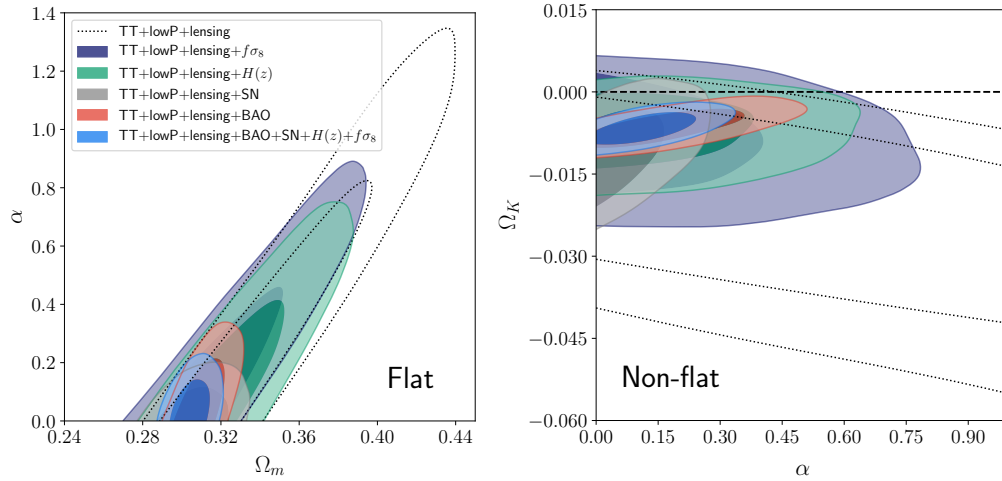


Figure 9. 1σ and 2σ likelihood contours in the Ω_m - α plane for the tilted flat ϕ CDM model (left panel) and in the α - Ω_k plane for the untilted nonflat ϕ CDM model (right panel), constrained by using Planck CMB TT + lowP + lensing and non-CMB data sets. The horizontal dashed line in the right panel indicates $\Omega_k = 0$. The color scheme shown in the left panel governs the contours in both panels. However, for nonflat ϕ CDM model constrained with TT + lowP + lensing, the prior $h \geq 0.45$ has been applied.

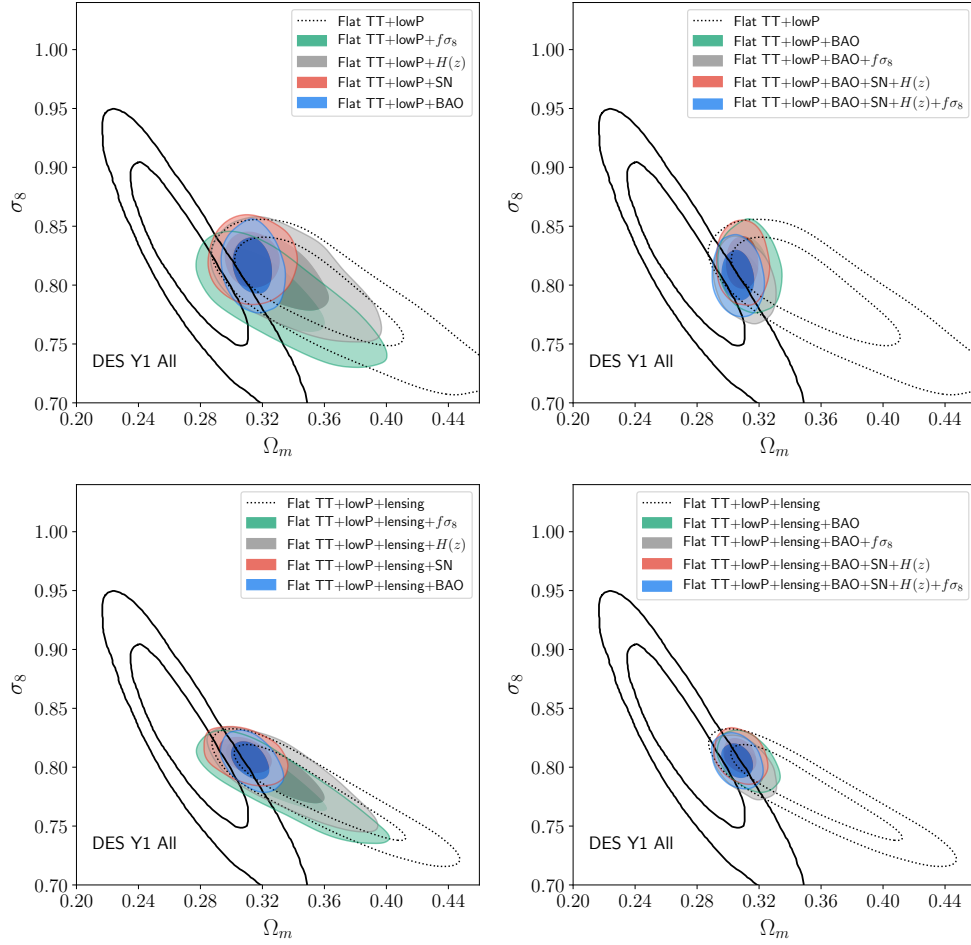


Figure 10. 1σ and 2σ likelihood contours in the Ω_m - σ_8 plane for the tilted flat ϕ CDM model parameters constrained by using Planck CMB TT + lowP (+lensing), SN, BAO, $H(z)$, and $f\sigma_8$ data. For comparison, in each panel the Λ CDM model 1σ and 2σ constraint contours from the first-year results of the Dark Energy Survey (DES Y1 All) (DES Collaboration 2017a) are plotted as thick solid curves.

ϕ CDM inflation model power spectra in Fig. 14 contributes to the TT power reduction at low- ℓ of the best-fit closed untilted model C_ℓ 's (see Figs. 12 and 13 lower panels) relative to the best-fit flat tilted model C_ℓ 's.²² The most dramatic case is that of the best-fit untilted nonflat ϕ CDM model for the TT + lowP data, consistent with the low- ℓ TT power reduction (Figs. 12b).²³

5. CONCLUSION

We have used the flat tilted and the nonflat untilted ϕ CDM dynamical dark energy inflation models to measure cosmological parameters from a reliable, large compilation of observational data.

Our main findings, in summary, are:

- We confirm, but at a lower significance of 0.40σ , the result of Ooba et al. (2018c) that the flat tilted ϕ CDM model better fits the data than does the standard flat tilted Λ CDM model. While the improvement is not significant, it does mean that current data allow for the possibility that dark energy is dynamical.
- In the nonflat untilted ϕ CDM case, we confirm, with greater significance, the Ooba et al. (2018b) result that cosmological data does not require flat spatial hypersurfaces for this model, and that the nonflat untilted ϕ CDM model better fits (at 0.93σ) the data than does the nonflat untilted Λ CDM model (qualitatively the standard flat tilted Λ CDM model provides a better fit to the data than does the nonflat untilted Λ CDM model). In the nonflat untilted ϕ CDM model, these data (including CMB lensing data) favor a closed model at more than 3.1σ significance, in which spatial curvature contributes a little less than two-thirds of a percent of the cosmological energy budget now.
- H_0 is measured here in a manner that is almost model-independent and is consistent with many other H_0 measurements. However, as is well known, an estimate of H_0 from the local expansion rate (Riess et al. 2018) is about 3.3σ larger.
- σ_8 here is measured in an almost model-independent manner and is consistent with the recent DES estimate (DES Collaboration 2017a).
- The value of Ω_m is more model dependent than the value of σ_8 and the Ω_m value measured using the nonflat untilted ϕ CDM model is more consistent with the recent DES estimate (DES Collaboration 2017a).
- $\Omega_c h^2$, τ , and a few of the other cosmological parameter values are quite model dependent.

²² The usual and integrated Sachs-Wolfe effects, as well as other effects, also play a role in determining the shape of the low- ℓ C_ℓ 's.

²³ Figure 24 (bottom-right panel) of Planck Collaboration (2018) shows the primordial power spectrum derived from the Planck CMB data. (We note that their Fig. 24 has been derived under the assumption that space is flat, and consequently ignores the effect of the spatial curvature Sachs-Wolfe and Integrated Sachs-Wolfe effects on the CMB power spectra that were used in the derivation of this figure.) This power spectrum is a power law over wavenumbers in the interval $5 \times 10^{-3} \lesssim k [\text{Mpc}^{-1}] \lesssim 2 \times 10^{-1}$ but at smaller wavenumbers their power spectrum amplitude errors are much larger and the Planck power spectrum is not inconsistent with our closed model power spectra plotted in Fig. 14.

These results are very similar to those for the XCDM dynamical dark energy parameterization presented in Park & Ratra (2018b).

We acknowledge valuable discussions with J. Ooba. C.-G.P. was supported by research funds of Chonbuk National University in 2017 and the Basic Science Research Program through the National Research Foundation of Korea (NRF) funded by the Ministry of Education (No. 2017R1D1A1B03028384). B.R. was supported in part by DOE grant DE-SC0019038.

REFERENCES

- Addison, G. E., Huang, Y., Watts, D. J., et al. 2016, ApJ, 818, 132 [arXiv:1511.00055]
- Alam, S., Ata, M., Bailey, S., et al. 2017, MNRAS, 470, 2617 [arXiv:1607.03155]
- Ata, M., Baumgarten, F., Bautista, J., et al. 2018, MNRAS, 473, 4773 [arXiv:1705.06373]
- Audren, B., Lesgourgues, J., Benabed, K., & Prunet, S. 2013, JCAP, 1302, 001 [arXiv:1210.7183]
- Avsajanishvili, O., Samushia, L., Arhipova, N. A., & Kahniashvili, T. 2015, arXiv:1511.09317
- Aylor, K., Hou, Z., Knox, L., et al. 2017, ApJ, 850, 101 [arXiv:1706.10286]
- Betoule, M., Kessler, R., Guy, J., et al. 2014, A&A, 568, A22 [arXiv:1401.4064]
- Blas, D., Lesgourgues, J., & Tram, T. 2011, JCAP, 1107, 034 [arXiv:1104.2933]
- Brax, P. 2018, Rep. Prog. Phys., 81, 016902
- Brax, P., Martin, J., & Riazuelo, A. 2000, Phys. Rev. D, 62, 103505 [arXiv:astro-ph/0005428]
- Cai, R.-G., Guo, Z.-K., & Yang, T. 2016, Phys. Rev. D, 93, 043517 [arXiv:1509.06283]
- Campanelli, L., Fogli, G.-L., Kahniashvili, T., Marrone, A., & Ratra, B. 2012, Eur. Phys. J., C72, 2218 [arXiv:1110.2310]
- Cao, S.-L., Duan, X.-W., Meng, X.-L., & Zhang, T.-J. 2018, Eur. Phys. J., C78, 313 [arXiv:1712.01703]
- Capozziello, S., Farooq, O., Luongo, O., & Ratra, B. 2014, Phys. Rev. D, 90, 044016 [arXiv:1403.1421]
- Challinor, A., & Lasenby, A. 1999, ApJ, 513, 1 [arXiv:astro-ph/9804301]
- Chen, G., Gott, J. R., & Ratra, B. 2003, PASP, 115, 1269 [arXiv:astro-ph/0308099]
- Chen, G., & Ratra, B. 2011a, PASP, 123, 1127 [arXiv:1105.5206]
- Chen, Y., Kumar, S., & Ratra, B. 2017, ApJ, 835, 86 [arXiv:1606.07316]
- Chen, Y., & Ratra, B. 2011b, Phys. Lett. B, 703, 406 [arXiv:1106.4294]
- Chen, Y., Ratra, B., Biesiada, M., Li, S., & Zhu, Z.-H. 2016, ApJ, 829, 61 [arXiv:1603.07115]
- da Silva, G. P., & Cavalcanti, A. G. 2018, arXiv:1805.06849
- DES Collaboration, Abbott, T. M. C., Abdalla, F. B., Alarcon, A., et al. 2017a, arXiv:1708.01530
- DES Collaboration, Abbott, T. M. C., Abdalla, F. B., Annis, J., et al. 2017b, arXiv:1711.00403
- Dhawan, S., Jha, S. W., & Leibundgut, B. 2017, A&A, 609, A72 [arXiv:1707.00715]
- Ding, X., Biesiada, M., Cao, S., Li, Z., & Zhu, Z.-H. 2015, ApJ, 803, L22 [arXiv:1503.04923]
- Farooq, O., Crandall, S., & Ratra, B. 2013, Phys. Lett. B, 726, 72 [arXiv:1305.1957]
- Farooq, O., Madiyar, F. R., Crandall, S., & Ratra, B. 2017, ApJ, 835, 26 [arXiv:1607.03537]
- Farooq, O., Mania, D., & Ratra, B. 2015, ApSS, 357, 11 [arXiv:1308.0834]
- Farooq, O., & Ratra, B. 2013, ApJ, 766, L7 [arXiv:1301.5243]
- Fernández Arenas, D., Terlevich, E., Terlevich, R., et al. 2018, MNRAS, 474, 1250 [arXiv:1710.05951]
- Gómez-Valent, A., & Amendola, L. 2018, JCAP, 0804, 051 [arXiv:1802.01505]
- Gómez-Valent, A., & Solà, J. 2017, Europhys. Lett., 120, 39001 [arXiv:1711.00692]
- Gómez-Valent, A., & Solà, J. 2018, arXiv:1801.08501
- Gott, J. R. 1982, Nature, 295, 304
- Gott, J. R., Vogeley, M. S., Podariu, S., & Ratra, B. 2001, ApJ, 549, 1 [arXiv:astro-ph/0006103]
- Haridasu, B. S., Luković, V. V., Moresco, M., & Vittorio, N. 2018b, arXiv:1805.03595
- Haridasu, B. S., Luković, V. V., & Vittorio, N. 2018a, JCAP, 1805, 033 [arXiv:1711.03929]
- Hawking, S. W. 1984, Nucl. Phys. B, 239, 257
- Hu, W., & Sugiyama, N. 1996, ApJ, 471, 542 [arXiv:astro-ph/9510117]
- Hwang, J., & Noh, H. 2001, Phys. Rev. D, 64, 103509 [arXiv:astro-ph/0108197]

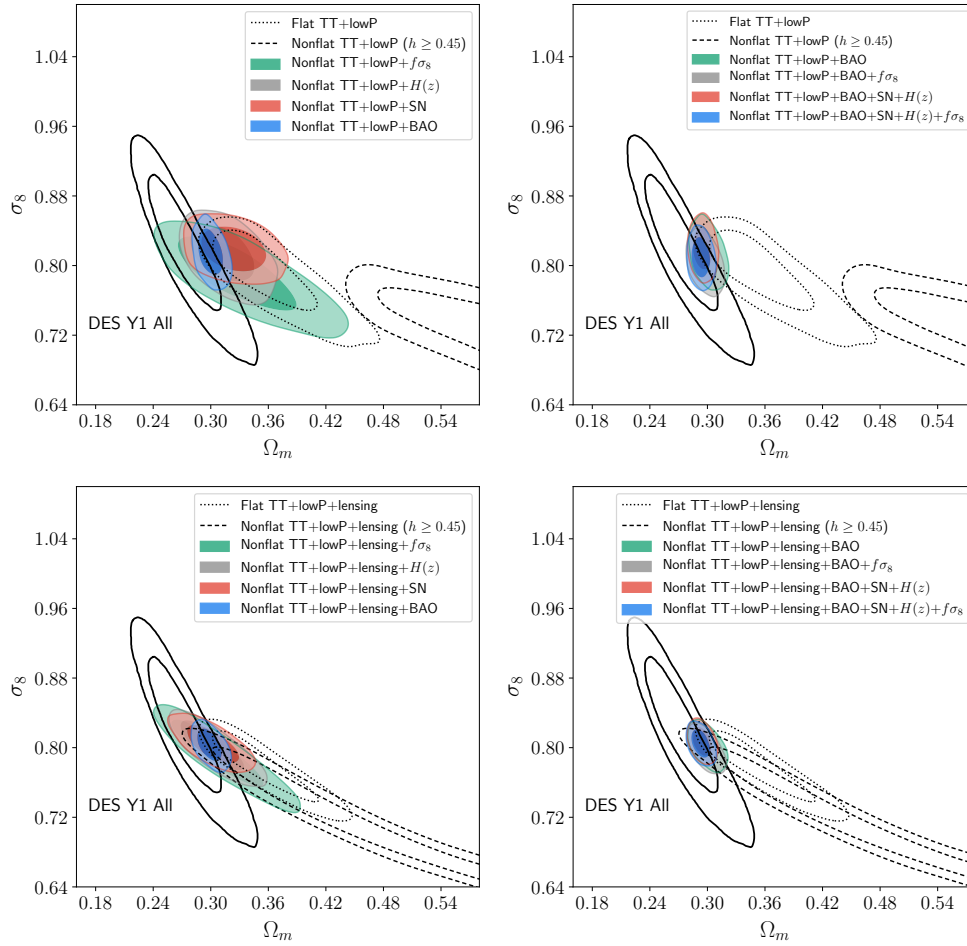


Figure 11. Same as Fig. 10 but for the untilted nonflat ϕ CDM model.

- Hwang, J., & Noh, H. 2002, Phys. Rev. D, 65, 023512 [arXiv:astro-ph/0102005]
- Jesus, J. F., Holanda, R. F. L., & Pereira, S. H. 2018, JCAP, 1805, 073 [arXiv:1712.01075]
- Jones, D. O., Riess, A. G., Scolnic, D. M., et al. 2018, arXiv:1805.05911
- Kim, Y.-L., Smith, M., Sullivan, M., & Lee, Y.-W. 2018, arXiv:1801.01192
- Lewis, A., & Bridle, S. 2002, Phys. Rev. D, 66, 103511 [arXiv:astro-ph/0205436]
- Lewis, A., Challinor, A., & Lasenby, A. 2000, ApJ, 538, 473 [arXiv:astro-ph/9911177]
- L'Huillier, B., & Shafieloo, A. 2017, JCAP, 1701, 015 [arXiv:1606.06832]
- Li, Z., Wang, G.-J., Liao, K., & Zhu, Z.-H. 2016, ApJ, 833, 240 [arXiv:1611.00359]
- Lin, W., & Ishak, M. 2017, Phys. Rev. D, 96, 083532 [arXiv:1708.09813]
- Lucchin, F., & Matarrese, S. 1985, Phys. Rev. D, 32, 1316
- Luković, V. V., D'Agostino, R., & Vittorio, N. 2016, A&A, 595, A109 [arXiv:1607.05677]
- Luković, V. V., Haridasu, B. S., & Vittorio, N. 2018, arXiv:1801.05765
- Martin, J. 2012, C. R. Physique, 13, 566 [arXiv:1205.3365]
- Mitra, S., Choudhury, T. R., & Ratra, B. 2018, MNRAS, 479, 4566 [arXiv:1712.00018]
- Moresco, M., Pozzetti, L., Cimatti, A., et al. 2016, JCAP, 1605, 014 [arXiv:1601.01701]
- Ooba, J., Ratra, B., & Sugiyama, N. 2018a, ApJ, 864, 80 [arXiv:1707.03452]
- Ooba, J., Ratra, B., & Sugiyama, N. 2017, arXiv:1710.03271
- Ooba, J., Ratra, B., & Sugiyama, N. 2018b, ApJ, in press [arXiv:1712.08617]
- Ooba, J., Ratra, B., & Sugiyama, N. 2018c, arXiv:1802.05571
- Park, C.-G., Lee, J.-h., Hwang, J.-c., & Noh, H. 2014 Phys. Rev. D, 90, 083526 [arXiv:1407.1512]
- Park, C.-G., & Ratra, B. 2018a, arXiv:1801.00213
- Park, C.-G., & Ratra, B. 2018b, arXiv:1803.05522
- Park, C.-G., & Ratra, B. 2018c, arXiv:1809.03598
- Pavlov, A., Westmoreland, S., Saaidi, K., & Ratra, B. 2013, Phys. Rev. D, 88, 123513 [arXiv:1307.7399]
- Peebles, P. J. E. 1984, ApJ, 284, 439
- Peebles, P. J. E., & Ratra, B. 1988, ApJ, 325, L17
- Penton, J., Peyton, J., Zahoor, A., & Ratra, B. 2018, PASP, 130, 114001 [arXiv:1808.01490]
- Planck Collaboration, Ade, P. A. R., Aghanim, N., Arnaud, M., et al. 2016, A&A, 594, A13 [arXiv:1502.01589]
- Planck Collaboration, Aghanim, N., Akrami, Y., Ashdown, M., et al. 2017, A&A, 607, A95 [arXiv:1608.02487]
- Planck Collaboration, Akrami, Y., Arroja, F., Ashdown, M., et al. 2018, arXiv:1807.06205
- Rana, A., Jain, D., Mahajan, S., & Mukherjee, A. 2017, JCAP, 1703, 028 [arXiv:1611.07196]
- Ratra, B. 1985, Phys. Rev. D, 31, 1931
- Ratra, B. 1989, Phys. Rev. D, 40, 3939
- Ratra, B. 1992, Phys. Rev. D, 45, 1913
- Ratra, B. 2017, Phys. Rev. D, 96, 103534 [arXiv:1707.03439]
- Ratra, B., & Peebles, P. J. E. 1988, Phys. Rev. D, 37, 3406
- Ratra, B., & Peebles, P. J. E. 1994, ApJ, 432, L5
- Ratra, B., & Peebles, P. J. E. 1995, Phys. Rev. D, 52, 1837
- Ratra, B., & Vogeley, M. 2008, PASP, 120, 235 [arXiv:0706.1565]
- Riess, A. G., Casertano, S., Yuan, E., et al. 2018, ApJ, 855, 136 [arXiv:1801.01120]
- Rigault, M., Aldering, G., Kowalski, M., et al. 2015, ApJ, 802, 20 [arXiv:1412.6501]
- Roman, M., Hardin, D., Betoule, M., et al. 2017, arXiv:1706.07697
- Ryan, J., Doshi, S., & Ratra, B. 2018, MNRAS, 480, 759 in press [arXiv:1805.06408]
- Sahni, V., Shafieloo, A., & Starobinsky, A. A. 2014, ApJ, 793, L4 [arXiv:1406.2209]
- Samushia, L., Chen, G., & Ratra, B. 2007, arXiv:0706.1963
- Samushia, L., & Ratra, B. 2010, ApJ, 714, 1347 [arXiv:0905.3836]
- Sangwan, A., Tripathi, A., & Jassal, H. K. 2018, arXiv:1804.09350
- Scolnic, D. M., Jones, D. O., Rest, A., et al. 2017, arXiv:1710.00845
- Seager, S., Sasselov, D. D., & Scott, D. 1999, ApJ, 523, L1 [astro-ph/9909275]
- Sołà, J., de Cruz Pérez, J., & Gómez-Valent, A. 2018, Europhys. Lett., 121, 39001 [arXiv:1606.00450]

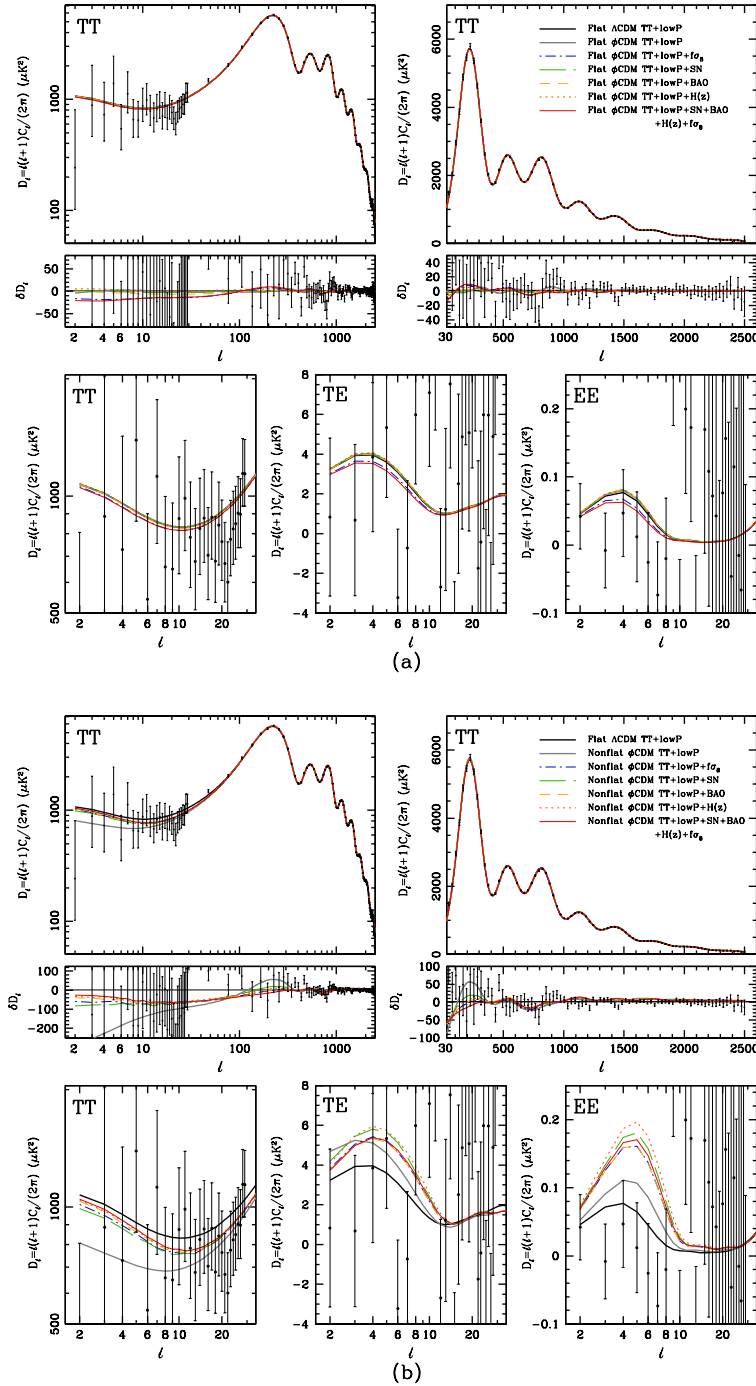


Figure 12. Best-fit CMB anisotropy angular power spectra of (a) flat tilted (top five panels) and (b) nonflat untitled ϕ CDM models (bottom five panels) constrained by using the Planck 2015 CMB TT + lowP data (ignoring the lensing data) in conjunction with BAO, $H(z)$, SN, and $f\sigma_8$ data. For comparison, the best-fit angular power spectra of the flat tilted Λ CDM model are shown as black curves. δD_{ℓ} residuals for the TT power spectra are shown with respect to the flat tilted Λ CDM power spectrum that best fits the TT + lowP data.

Table 5
Individual and total χ^2 values for the best-fit tilted flat and untilted nonflat ϕ CDM inflation models.

Data sets	χ^2_{Planck}	χ^2_{lowTEB}	χ^2_{lensing}	χ^2_{SN}	χ^2_{BAO}	$\chi^2_{H(z)}$	$\chi^2_{f\sigma_8}$	χ^2_{prior}	Total χ^2	$\Delta\chi^2$
Tilted flat ϕ CDM model										
TT+lowP	766.02	10496.47						0.24	11262.25	+0.32
+SN	763.68	10496.29		1036.31				2.01	12298.30	-0.01
+BAO	764.40	10495.97			12.85			1.95	11275.18	-0.07
+ $H(z)$	763.35	10496.70				14.93		1.88	11276.86	-0.07
+ $f\sigma_8$	766.75	10494.91					12.13	1.96	11275.75	-0.05
+BAO+ $f\sigma_8$	767.30	10494.94			12.04		11.99	1.98	11288.25	-0.25
+SN+BAO	764.23	10496.03		1036.12	12.94			2.03	12311.36	-0.05
+SN+BAO+ $H(z)$	764.23	10496.04		1036.16	12.96	14.82		2.01	12326.21	+0.00
+SN+BAO+ $H(z)$ + $f\sigma_8$	766.85	10494.80		1036.07	12.57	14.79	12.05	2.11	12339.24	-0.12
TT+lowP+lensing	766.47	10495.03	9.24					2.05	11272.79	+0.35
+SN	766.31	10494.80	9.21	1036.07				2.13	12308.51	-0.08
+BAO	767.08	10494.69	9.06		12.29			1.88	11285.00	-0.07
+ $H(z)$	766.28	10494.84	9.21			14.84		2.09	11287.26	-0.01
+ $f\sigma_8$	767.53	10494.57	8.74				11.54	2.20	11284.58	-0.04
+BAO+ $f\sigma_8$	767.84	10494.56	8.69		12.05		11.63	2.18	11296.95	-0.37
+SN+BAO	766.37	10494.80	9.16	1036.10	12.60			2.10	12321.14	-0.03
+SN+BAO+ $H(z)$	766.71	10494.74	9.17	1036.21	12.49	14.83		1.94	12336.08	+0.07
+SN+BAO+ $H(z)$ + $f\sigma_8$	767.76	10494.53	8.70	1036.13	12.44	14.79	11.60	2.08	12348.04	-0.16
Untilted nonflat ϕ CDM model										
TT+lowP	773.80	10496.68						1.88	11272.36	+0.26
+SN	776.52	10498.66		1036.99				1.86	12314.03	-0.91
+BAO	783.17	10497.33			13.52			1.86	11295.88	-0.20
+ $H(z)$	778.01	10500.10				17.30		1.83	11297.23	+0.08
+ $f\sigma_8$	781.56	10497.32					12.66	1.85	11293.39	-1.40
+BAO+ $f\sigma_8$	782.60	10499.20			12.24		10.94	1.74	11306.72	-0.69
+SN+BAO	782.64	10498.87		1036.17	12.54			1.91	12332.13	-0.17
+SN+BAO+ $H(z)$	782.77	10498.26		1036.05	12.63	15.73		2.07	12347.52	-1.05
+SN+BAO+ $H(z)$ + $f\sigma_8$	783.46	10498.06		1036.24	12.22	15.62	11.02	2.18	12358.81	-1.17
TT+lowP+lensing	789.84	10495.16	8.60					1.22	11292.37	+0.08
+SN	786.79	10493.86	9.83	1036.12				1.72	12328.32	+0.01
+BAO	784.96	10498.48	8.82		11.39			2.05	11305.69	-1.71
+ $H(z)$	785.54	10497.28	8.84			15.35		1.80	11308.81	-1.29
+ $f\sigma_8$	787.33	10495.34	8.64				10.05	1.71	11303.07	+0.14
+BAO+ $f\sigma_8$	785.85	10498.06	8.53		11.50		9.77	2.02	11315.73	-1.58
+SN+BAO	783.34	10499.33	9.65	1036.67	11.77			1.84	12342.59	-0.20
+SN+BAO+ $H(z)$	785.03	10498.28	8.99	1036.79	11.78	15.38		1.80	12358.05	-0.82
+SN+BAO+ $H(z)$ + $f\sigma_8$	786.41	10497.91	8.46	1036.65	11.98	15.36	9.38	1.84	12368.00	-0.86

Note: $\Delta\chi^2$ of tilted flat or untilted nonflat ϕ CDM model represents the excess value relative to χ^2 of the tilted flat or untilted nonflat Λ CDM model estimated for the same combination of data sets (listed in Table 7 of [Park & Ratra 2018b](#)).

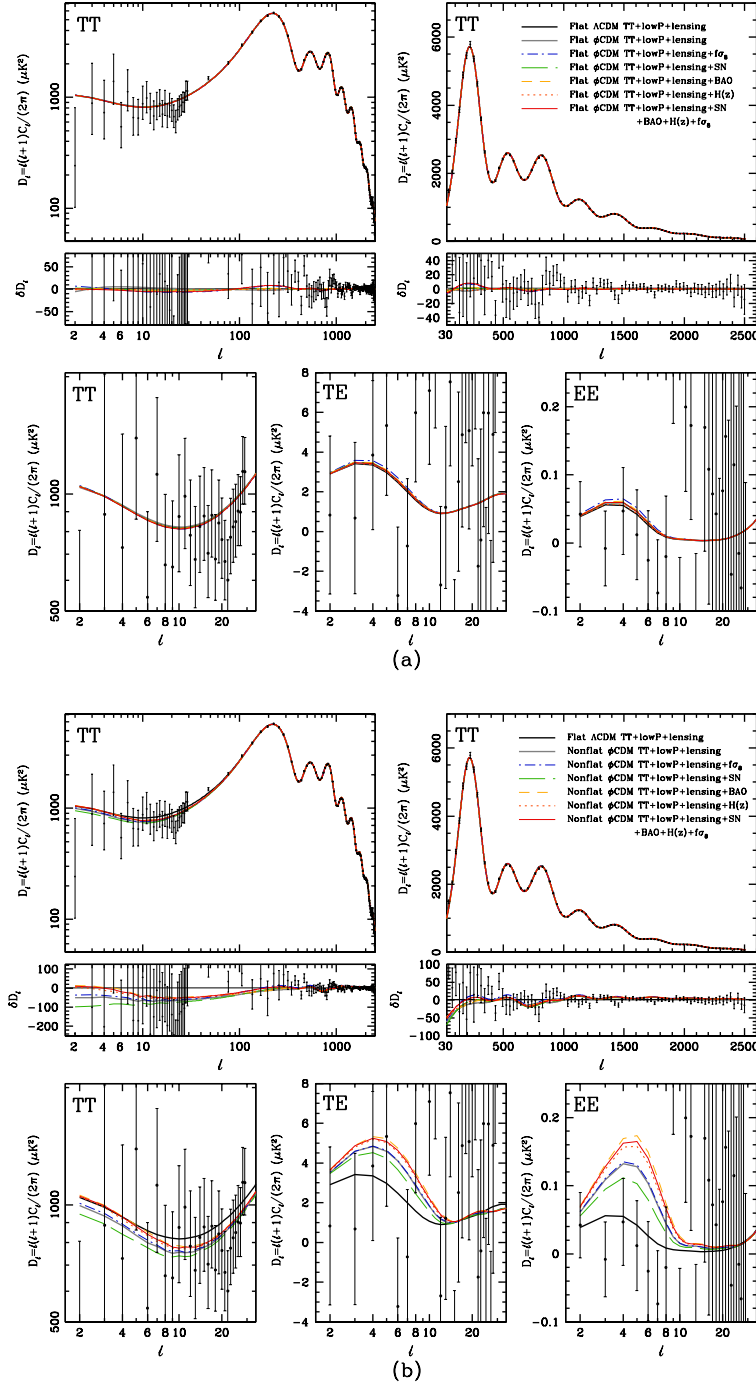


Figure 13. Same as Fig. 12 but now accounting for the CMB lensing data. δD_ℓ residuals of the TT power spectra are shown with respect to the flat tilted Λ CDM power spectrum that best fits the TT + lowP + lensing data.

Solà, J., de Cruz Pérez, J., & Gómez-Valent, A. 2017c, arXiv:1703.08218
 Solà, J., Gómez-Valent, A., & de Cruz Pérez, J. 2015, ApJ, 811, L14 [arXiv:1506.05793]
 Solà, J., Gómez-Valent, A., & de Cruz Pérez, J. 2017a, ApJ, 836, 43 [arXiv:1602.02103]
 Solà, J., Gómez-Valent, A., & de Cruz Pérez, J. 2017b, Mod. Phys. Lett. A, 32, 1750054 [arXiv:1610.08965]
 Solà, J., Gómez-Valent, A., & de Cruz Pérez, J. 2017d, Phys. Lett. B, 774, 317 [arXiv:1705.06723]
 Wang, Y., Xu, L., & Zhao, G.-B. 2017, ApJ, 849, 84 [arXiv:1706.09149]
 Wei, J.-J., & Wu, X.-F. 2017, ApJ, 838, 160 [arXiv:1611.00904]

Wong, W. Y., Moss, A., & Scott, D. 2008, MNRAS, 386, 1023 [arXiv:0711.1357]
 Yashar, M., Bozek, B., Abrahamse, A., Albrecht, A., & Barnard, M. 1999, Phys. Rev. D, 79, 103004 [arXiv:0811.2253]
 Yu, H., Ratra, B., & Wang, F.-Y. 2018, ApJ, 856, 3 [arXiv:1711.03437]
 Yu, H., & Wang, F. Y. 2016, ApJ, 828, 85 [arXiv:1605.02483]
 Zhai, Z., Blanton, M., Slosar, A., & Tinker, J. 2017, ApJ, 850, 183 [arXiv:1705.10031]
 Zhang, B. R., Childress, M. J., Davis, T. M., et al. 2017b, MNRAS, 471, 2254 [arXiv:1706.07573]
 Zhang, J. 2018, PASP, 130, 084502
 Zhang, X., Huang, Q.-G., & Li, X.-D. 2018, arXiv:1801.07403

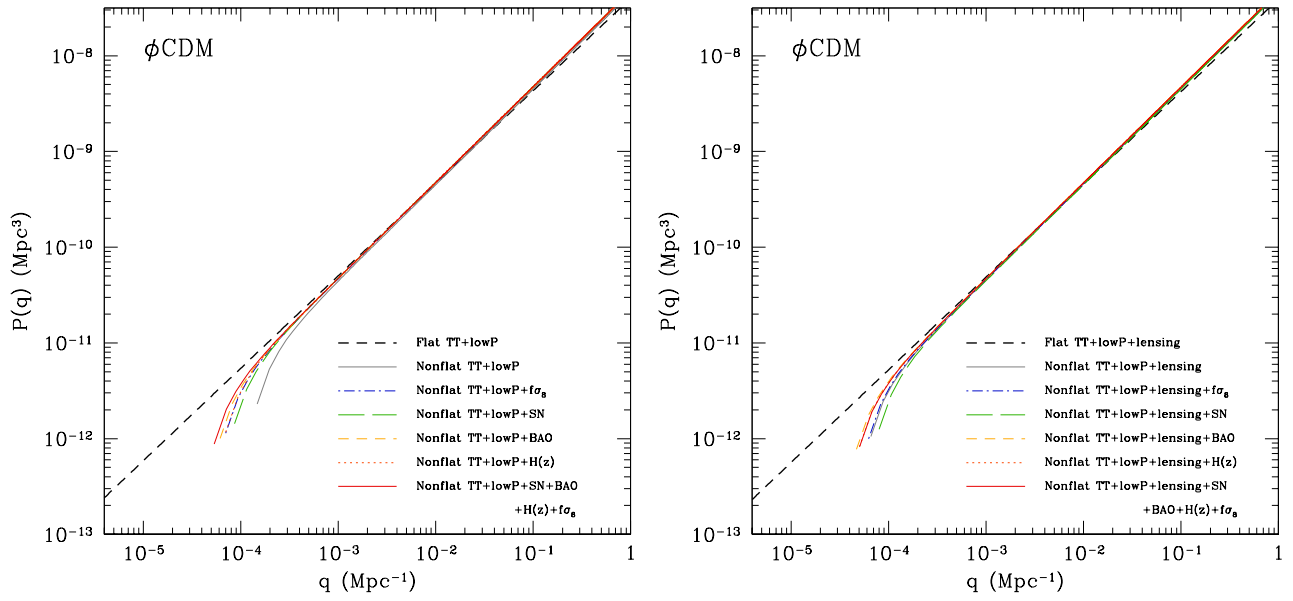


Figure 14. Primordial scalar-type perturbation power spectra with non-power-law form of the best-fit untilted nonflat ϕ CDM models constrained with Planck TT + lowP (left panel) and TT + lowP + lensing data (right panel) together with SN, BAO, $H(z)$, $f\sigma_8$ non-CMB data sets. In both panels the primordial power spectrum of the best-fit tilted flat ϕ CDM model is shown as dashed lines. See Sec. 3 for the definition of q . Note that all power spectra are normalized to $P(q) = A_s$ at $k_0 = 0.05 \text{ Mpc}^{-1}$.

Zhang, Y.-C., Zhang, H.-Y., Wang, D.-D., et al. 2017a, Res. Astron. Astrophys., 17, 6 [arXiv:1703.08293]
Zhao, G.-B., Raveri, M., Pogosian, L., et al. 2017, Nat. Astron., 1, 627 [arXiv:1701.08165]

Zheng, X., Ding, X., Biesiada, M., Cao, S., & Zhu, Z.-H. 2016, ApJ, 825, 17 [arXiv:1604.07910]